ACKNOWLEDGEMENTS

First of all, I would like to thank my supervisor Professor Anders Holmen, for his support, encouragement and excellent guidance throughout my work.

Special thanks go to my co-supervisor Professor De Chen, for his invaluable enlightening ideas, discussions, and experimental help throughout the project.

Associate Professor Bård Tøtdal at the Department of Physics is gratefully acknowledged for his enthusiastic help with the TEM experiments.

John Rasmus Leinum and Elin Nilsen, both at the Department of Material Technology, are acknowledged for SEM and XRD. Professor Steinar Raaen at the Department of Physics is acknowledged for XPS. Associate Professor Magnus Rønning, Torbjørn Vrålstad, and Esther Ochoa-Fernández are acknowledged for EXAFS. Ingvar Kvande and Esther Ochoa-Fernández are also acknowledged for experimental help and discussions. Dr. Edvard Bergene, and Asbjørn Lindvåg at SINTEF are acknowledged for technical assistance.

Our collaborators at State Key Laboratory of Chemical Reaction Engineering, East China University of Science and Technology are thanked for their contributions on various aspects.

My colleagues at the Catalysis group are highly appreciated for their support and friendship.

The financial support from the Research Council of Norway, the Department of Chemical Engineering, and Statoil is gratefully acknowledged.

Finally, my family deserves many thanks for their endless patience, support, and encouragement.

ABSTRACT

Carbon nanofibers (CNFs) and carbon nanotubes (CNTs) have attracted intense research efforts with the expectation that these materials may have many unique properties and potential applications. The most promising way for large-scale synthesis of CNFs and CNTs is chemical vapor deposition (CVD).

CNFs were synthesized on a series of hydrotalcite (HT) derived 77 wt.% Ni-Fe/Al_2O_3 catalysts in order to achieve the optimization of productivity and quality. It was found that only the Fe catalyst was active in CO disproportionation and only the Ni catalyst was active in ethylene decomposition, whereas all catalysts were active in ethylene decomposition when the reactants were a mixture of C_2H_4/CO. More control over the structure and diameter of the CNFs has been realized with the HT catalysts. At the same time, a high yield can be obtained. The synthesis process has been further studied as a function of various process parameters. It turned out that high hydrogen concentration, space velocity, and reaction temperature would enhance the production of CNFs. However, a slightly lower quality was associated with the higher productivity. The optimum CNF yield of 128 gCNF/gcat could be reached within 8 h on the HT catalyst with a Ni/Fe ratio of 6:1. Therefore, HT derived catalysts present a new promising route to large-scale controlled synthesis of CNFs.

CNTs has been synthesized from CO disproportionation on Ni-Fe/Al_2O_3 supported catalysts with metal loadings of 20 and 40 wt.%. A high space velocity resulted in a high production rate but a short lifetime and a low carbon capacity. Increasing the metal loading to 40 wt.% significantly increased the reaction rate and productivity, and produced similarly uniform CNTs. Furthermore, H_2 was found to be necessary for a high productivity, and the H_2 partial pressure could be changed to adjust the orientation angle of the graphite sheets.

The effects of catalyst particle size and catalyst support on the CNT growth rate during CO disproportionation were studied over SiO_2 and Al_2O_3 supported Fe catalysts with varying particle sizes. It was found that there was an optimum particle size at around 13-15 nm for the maximum growth rate, and the growth rate was influenced both by the particle size and the support but the particle size was the dominating factor. The trends have been demonstrated at two different synthesis temperatures of 600 and 650°C.

The effect of gas precursors on the yield and structure of carbon growth has been systematically investigated over powder Fe and Fe/Al_2O_3 catalysts. CO/H_2, CO, CH_4, and C_2H_6/H_2 were the gas precursors studied. The carbon yield was higher on powder Fe from CO, but the yield was higher on Fe/Al_2O_3 from hydrocarbons. Completely different or similar carbon nanostructures were synthesized, depending on the gas precursors. It was suggested that the reactivity of gas precursors and the structures of carbon deposits are determined by the size and crystallographic faces of the catalyst particles, which are dictated by the interactions among metal particles, support, and the reactants. Controlled synthesis of CNT, platelet nanofiber, fishbone-tubular nanofiber, and onion-like carbon with high selectivity and yield was realized. A mechanism was proposed to illustrate the growth of different carbon nanostructures.

LIST OF PUBLICATIONS AND PRESENTATIONS

List of publications

I. Zhixin Yu, Torbjørn Vrålstad, Magnus Rønning, Esther Ochoa-Fernández, De Chen, and Anders Holmen: Large-Scale Synthesis of Carbon Nanofibers over Ni-Fe Hydrotalcite Derived Catalysts. I: Preparation and Characterization of the Ni-Fe Hydrotalcites. To be submitted.

II. Zhixin Yu, Bård Tøtdal, Magnus Rønning, Esther Ochoa-Fernández, Torbjørn Vrålstad, De Chen, and Anders Holmen: Large-Scale Synthesis of Carbon Nanofibers over Ni-Fe Hydrotalcite Derived Catalysts. II: Effect of Ni/Fe Composition on CNF Synthesis. To be submitted.

III. Zhixin Yu, De Chen, Bård Tøtdal, and Anders Holmen: Parametric Study of Carbon Nanofiber Growth by Catalytic Ethylene Decomposition on Hydrotalcite Derived Catalysts. Materials Chemistry and Physics, in press.

IV. Zhixin Yu, De Chen, Bård Tøtdal, Tiejun Zhao, Yingchun Dai, Weikang Yuan, and Anders Holmen: Catalytic Engineering of Large-Scale Carbon Nanotube Production. Applied Catalysis A 279 (2005) 223.

V. Zhixin Yu, De Chen, Bård Tøtdal, and Anders Holmen: Effect of Catalyst Preparation on the Carbon Nanotube Growth Rate. Catalysis Today, in press.

VI. Zhixin Yu, Ingvar Kvande, Tiejun Zhao, De Chen, Yingchun Dai, Weikang Yuan, and Anders Holmen: What Determines the Carbon Nanotube Growth Rate: Catalyst Support or Particle Size? Submitted.

VII. Zhixin Yu, De Chen, Bård Tøtdal, and Anders Holmen: Effect of Support and Reactant on the Growth and Structure of Carbon Deposits by Chemical Vapor Deposition. Journal of Physical Chemistry B, in press.

This thesis is based on the above seven papers.

Additional publications

VIII. De Chen, Kjersti O. Christensen, Esther Ochoa-Fernández, Zhixin Yu, Bård Tøtdal, Nieves Latorre, Antonio Monzón, and Anders Holmen: Synthesis of Carbon Nanofibers: Effects of Ni Crystal Size during Methane Decomposition. Journal of Catalysis 229 (2004) 87.

IX. Esther Ochoa-Fernández, De Chen, Zhixin Yu, Bård Tøtdal, Magnus Rønning, and Anders Holmen: Effect of Carbon Nanofiber-induced Microstrain on the Catalytic Activity of Ni Crystals. Surface Science 554 (2004) L107.

List of presentations at conferences

1. Zhixin Yu, De Chen, Bård Tøtdal, and Anders Holmen: Effect of Catalyst Preparation on the Carbon Nanotube Growth Rate. Oral presentation at 11th Nordic Symposium on Catalysis, Oulu, Finland, May 23-25, 2004.
2. Zhixin Yu, De Chen, Bård Tøtdal, and Anders Holmen: Role of the Catalyst Structure in Large-Scale Carbon Nanotube Synthesis on Fe Catalysts. Oral presentation at EUROMAT 2003, Lausanne, Switzerland, September 1-5, 2003.
3. De Chen, Esther Ochoa-Fernández, Ingvar Kvande, Zhixin Yu, and Anders Holmen: Preparation, Characterization, and Activity of Carbon Nanofiber Supported Ni Catalyst. Poster presentation at EuropaCat-VI, Innsbruck, Austria, September 2003.
4. De Chen, Zhixin Yu, Bård Tøtdal, and Anders Holmen: Carbon Nanofiber Production and Applications in (Electro)Catalysis. Oral presentation at

International Symposium on Electrocatalysis in Fuel Cell, Trondheim, Norway, May 5, 2003.

5. Tiejun Zhao, Xiongyi Gu, W. Wu, Yinchun Dai, WeikangYuan, De Chen, Zhixin Yu, and Anders Holmen: Large Scale Synthesis of Carbon Nanofibers in CO/H_2 Mixtures for Use as Composite Materials. Oral presentation at European Workshop on Carbon Nanotube/Nanofibre Reinforced Polymers, Cambridge, England, March 2003.
6. Zhixin Yu, De Chen, Bård Tøtdal, and Anders Holmen: Catalytic Growth of Carbon Nanofibers and the Characterization. Oral presentation at Norsk Katalysesymposium, Hafjell, Norway, November 28-29, 2002.
7. De Chen, Zhixin Yu, and Anders Holmen: Carbon Nanofiber Production and Application in Hydrogen Related Processes. Oral presentation at Norsk Hydrogenseminar, Trondheim, Norway, October 2002.
8. Zhixin Yu, De Chen, Bård Tøtdal, and Anders Holmen: Carbon Deposition on Ni-Fe Hydrotalcite-like Catalysts from Ethylene. Poster presentation at 2nd EFCATS School on Catalysis, Tihany, Hungary, September 25-29, 2002.

TABLE OF CONTENTS

1 INTRODUCTION

1.1 CNFs and CNTs, historical development

Carbon materials are found in variety forms such as graphite, diamond, fullerenes, carbon nanofibers (CNFs), and carbon nanotubes (CNTs). The new carbon allotrope, fullerene, was discovered by Kroto *et al*. [1] in 1985. It is a closed-cage carbon molecule with sp^2 carbon atoms, the best know being C_{60}. It was not until the discovery of CNTs by Iijima [2, 3], that the research in these new carbon materials has undergone an explosive growth in the past decades.

The origin of the concept of CNTs can be found in fullerenes and the traditional vapor grown carbon fibers (VGCFs). A single walled carbon nanotube (SWNT) may be considered as an elongated fullerene. For several decades there has been active research on carbon fibers [4, 5]. Very small diameter (less than 10 nm) carbon filaments were prepared in the 1970's and 1980's by the deposition of hydrocarbons at high temperatures in the presence of transition metal particles. These processes are not very different from the current chemical vapor deposition (CVD) method used for CNF and CNT synthesis [6].

These new nanocarbon materials have sparked a considerable amount of excitement for chemists, physicists, and materials scientist worldwide. The past decades have seen an exponential increase in patent filings and publications on CNTs (Figure 1.1). Research has shown that the nanotubes have superior mechanical, thermal, and electrical properties, making them unique for many applications. Smalley *et al.* [7] conjectured diverse applications, ranging from molecular composites to microelectronics to nanoprobes for chemical and biological applications to hydrogen storage devices. Some fascinating applications have already been demonstrated at the prototype stage, and future nanotechnologies in many areas could well be built on the advances that have been made for CNTs.

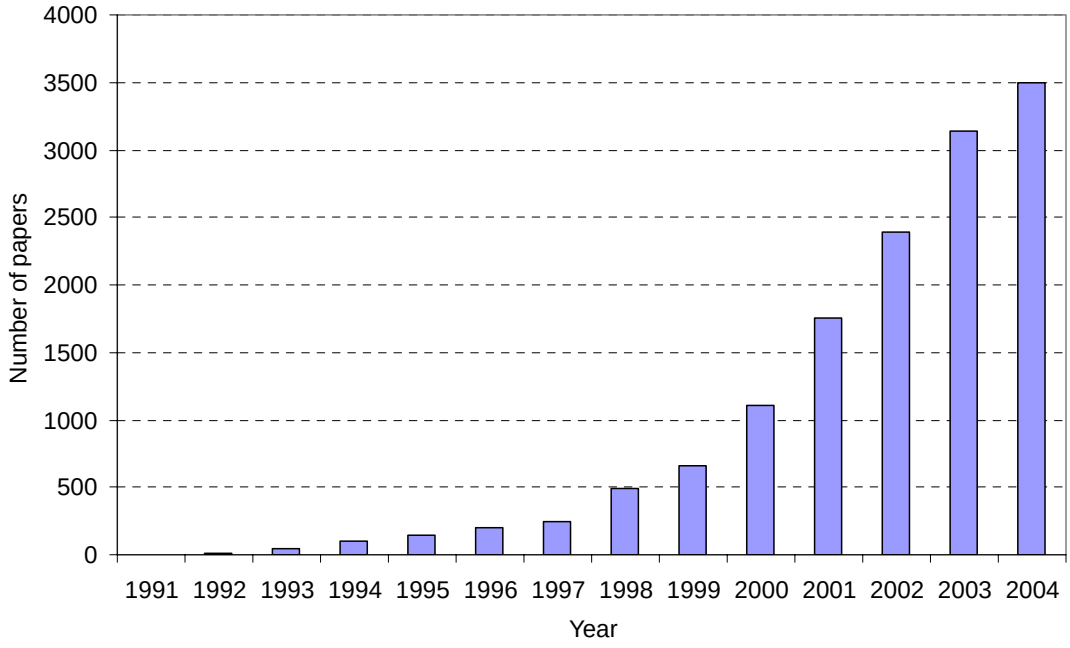

Figure 1.1. *Number of publications on CNTs during last decades (From SciFinder; In 1991 CNTs are called microtubules of graphitic carbon).*

1.2 Structures and properties

A SWNT can be seen as a graphite sheet (sometimes called graphene) rolled up into a cylinder with a typical diameter on the order of 1.4 nm (Figure 1.2). The sidewall of SWNTs consists of sp^2 hybridized carbon atoms that exhibit similar bonding and structure as graphite. A multi-walled carbon nanotube (MWNT) consists of concentric cylindrical layers of graphite sheets.

In addition to the cylindrical CNTs, there are also other types of the arrangement of graphite sheets. In a fishbone nanofiber the graphite sheets are stacked with an angle to the fiber axis. In a platelet nanofiber the graphite sheets are perpendicular to the fiber axis. In MWNTs or nanofibers, the interlayer distance is approximately 0.34 nm, close to the interlayer distance in graphite.

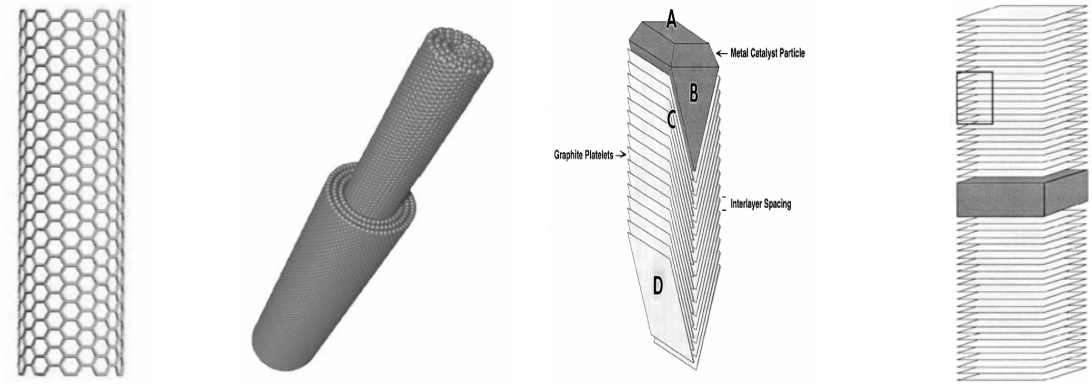

Figure 1.2. *Different carbon nanostructures (from left): SWNT, MWNT, fishbone nanofiber, and platelet nanofiber.*

The distinction between CNTs and CNFs by name is far from clear. Endo *et al.* [8] defined carbon fibers as a one-dimensional filament morphology consisting of sp^2 bonded graphitic carbon oriented along an axis parallel to the basal plane. This essentially defines CNTs. In this study CNTs or CNFs are distinguished according to the occurrence of a hollow core and the graphite sheets arrangement: those with a hollow core and with graphite sheets parallel to the axis are called CNTs, while others are classified as CNFs.

The different carbon nanostructures will exhibit major differences in their physical and chemical properties. CNFs will only have edge sites exposed, and they will be unstable because of the dangling bonds of the fiber edges, but will be ideal candidates for gas adsorption. The tubular structure will have their surface consisting primarily of basal planes and will have high electrical conductivity. The peculiar thermal, mechanical, and electrical properties are primarily associated with SWNTs.

1.3 Synthesis methods

Carbon nanostructures can be synthesized via three main processes: arc-discharge, laser ablation, or chemical vapor deposition (CVD). Apparatus for the three different processes is schematically displayed in Figure 1.3.

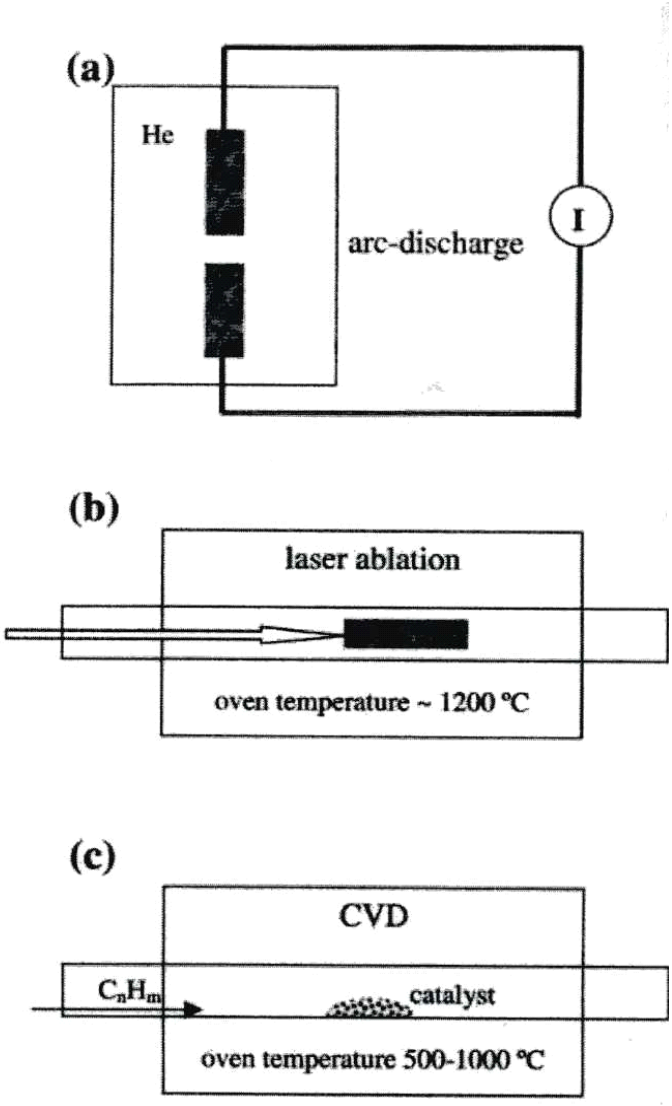

Figure 1.3. *Schematic representation of the CNT synthesis apparatus.*

In the arc-discharge process, a DC arc discharge between two graphite electrodes is ignited in an inert gas (Ar or He). The electric arc vaporizes a hollow graphite anode packed with a mixture of a transition metal (Fe, Co, or Ni) and graphite powder. This results in the consumption of one electrode forming different carbon nanostructures such as SWNT, MWNT, fullerenes. A large amount of soot and carbon nanoparticles are also formed. Arc discharge yields the most highly graphitized tubes because of the very high temperatures (2000-3000°C) [9]. The synthesis of MWNTs at the gram level by arc discharge was first achieved by Ebbesen *et al.* [10], and the first success in producing substantial amount of SWNTs was achieved by Bethune *et al.* [11].

In laser ablation, a graphite target mixed with a small amount of transition metal particles as catalyst is positioned at the end of a quartz tube enclosed in furnace. The target is exposed to a laser beam that vaporizes graphite and nucleates CNTs just in front of the target. Argon flow through the reactor heated to about 1200°C by the furnace carries the vapor. The nanotubes deposit at the cooler zone at the end of the tube furnace in the direction of the gas flow. This produces SWNTs and MWNTs with high yield, with the rest being catalyst particles and soot. The growth of high

quality SWNTs at the 1-10 gram scale by laser ablation was achieved firstly by Smalley *et al.* [12].

All kinds of carbon nanostructures can be synthesized employing the CVD method: a reactor is loaded with a metal catalyst and fed with a carbon-containing gas or gas mixture. The growth process involves heating the catalyst to moderate temperatures in the range of 500 to 1000°C in the furnace. Carbon is deposited on the catalyst surfaces.

The first two methods produce high-quality and nearly perfect nanotube structures, despite large amounts of byproducts. With regard to large-scale synthesis, the CVD route is by far the most feasible option in terms of cost and energy requirements. Nanotubes obtained by CVD are longer than those obtained by arc-discharge, although not as well crystallized and contain high densities of defects [13].

1.4 Scope of the present work

Our interests in CNFs and CNTs were initially in the application as hydrogen storage materials and as catalyst supports. For these applications a large amount of CNFs or CNTs is necessary. Therefore, synthesis of CNFs/CNTs with high productivity is a major purpose of the present study.

The properties and applications of CNFs and CNTs depend significantly on their structures. This study has aimed at tailoring the carbon filament structures by changing the reaction conditions and/or the catalyst precursors. It has also aimed at synthesizing CNFs and CNTs with high quality, small size and narrow size distribution, and good crystallinity, which are all desirable properties for applications. Therefore, an optimized CNF/CNT productivity and quality is another purpose of this study.

In addition, a hydrogen storage apparatus has been designed and built. Subsequent hydrogen storage experiments will be performed with this apparatus.

2 LITERATURE REVIEW

Few materials have elicited so many reviews as CNFs and CNTs. Some of the earlier reviews have described quite extensively various aspects of carbon fiber growth [14-18]. Recent comprehensive reviews on CNFs can be found by de Jong [19] and Chesnokov [20]. Extensive reviews [21-34] and several monographs [35-39] have also been published on CNTs.

As the present work mainly involves the synthesis of CNFs and CNTs by varying the catalyst precursors, catalyst supports, gas precursors, temperatures, *etc.*, the effects of these parameters on the growth characteristics, carbon yield, structure and quality of CNFs/CNTs have been focused in the following review. This was followed by a mechanistic description of the CVD growth process. Finally, the application as hydrogen storage materials is briefly summarized. Concerning the vast literatures on CNTs, the discussion will not be exhaustive, but only representative examples will be included.

2.1 CVD growth of CNFs/CNTs

The CVD process has appeared as the most promising method in CNF/CNT synthesis due to its relatively low cost and high yield production. It has been applied both in the absence and in the presence of a substrate. The former is a gas phase homogeneous process based on the decomposition of two precursors, one for the metal catalyst and the other for carbon. The latter is a heterogeneous process which uses either bulk catalysts or supported catalysts. Both processes appear very sensitive to the nature and structure of the catalytic system and to the operation conditions. The literature below is mainly based on the heterogeneous processes which have been explored much more intensively. Though, the conclusions should also give some insight on the homogeneous processes.

2.1.1 Powder catalysts vs supported catalysts

Baker and coworkers have undertaken extensive studies of CNF production using a series of unsupported mono and bimetallic catalyst powders [40-46]. Unsupported powder catalysts are highly efficient for a high CNF yield (up to 300gC/gcat) [47, 48], but lead mainly to the production of CNFs. Another major shortcoming of power catalysts is that one has little control over the size and structures of the final CNFs. This is mainly due to the uncontrolled changes of the catalyst precursors during the reduction and subsequent carbon growth processes. In order to produce small structured CNFs with a controlled size, it is necessary to disperse the metal catalyst particles on a suitable support [47].

Anderson *et al.* [49, 50] demonstrated that major modification in the growth of CNFs can be achieved when metals are used in a supported form than in a powder form. The use of support material generated CNFs with width dictated by the dimensions of the supported metal particles [49]. The support may also alter the precipitation faces of the catalyst particle, which in turn influences the structural characteristics of the CNFs. For example, CNFs grown from iron powder from CO/H_2 at 600°C possess a platelet structure, whereas CNFs grown on the silica supported iron possess a tubular structure [47].

Therefore, using supported catalysts is essential for the control of both the size and morphologies of the catalyst particles. Nevertheless, the use of supported catalysts suffers the problem of removal of the support without damage to the carbon. More seriously, only a low productivity can be achieved, most probably due to the low active metal loading, but also possibly due to the metal support interaction, which is not favored for a high carbon yield [51].

2.1.2 Catalyst supports

While powder and supported metals exhibit different reactivity and CNT growth characteristics, metals on different supports seem also to have different activity and CNT growth due to different nature and strength of the metal-support interactions. The effects have been manifested in many studies [51-55].

Park *et al.* [52] studied the catalyst support effects in the carbon growth from ethylene decomposition on supported Ni catalyst. It was found that the characteristics of CNFs generated can be readily manipulated by a judicious choice of the support materials. The occurrence and ramifications of Ni/support interactions, in terms of Ni particle size/morphology/orientation, are related to the carbon structure/dimensions and yield. de los Arcos *et al.* [55] found that formation of thin tubes and fast growth rate were associated with the underlying Al_2O_3 layer, whereas thick MWNTs were grown from Fe on the TiN and TiO_2 layers. The influence has been attributed to a combination of chemical and morphological changes induced in the catalyst due to the catalyst-substrate interaction.

The support may have impact on the product quality. Li *et al.* [56] found that MgO was the best for CNT synthesis from methane decomposition compared with other supports such as SiO_2, Al_2O_3, ZrO_2 and CaO.

The support effects have also been documented quite extensively by the B.Nagy group [57-60]. Interestingly, for acetylene and methylacetelene decomposition on supported Ni, Co, or Fe catalysts, Hernadi [60] disclosed that the catalyst supports have more influence on CNT selectivity than the metallic particle itself.

A good summary of the effects of metal-support interaction was given by Anderson *et al.* [49]: it induces electronic perturbations throughout the metal; it generates significant differences in metal morphology and the arrangement of the surface atoms; it exerts an influence of the growth characteristics of the supported metal particles; and it possibly modifies the chemistry of the system.

2.1.3 Catalyst precursors

The growth rate, diameter, and crystallinity of the CNTs can be manipulated by the selection of the catalyst precursors. Several studies have focused on supported Ni, Fe, Co catalysts for CNT growth from acetylene decomposition [61-64]. Lee *et al.* [61] used silicon support and found that the growth rate shows the order of Ni>Co>Fe. The average diameter follows the sequence of Fe, Co, and Ni. The structures of CNTs reveals almost same morphology regardless of catalyst but the crystallinity is better from Fe than Ni and Co. Soneda *et al.* [63] used MgO support and found that Co is the most effective catalyst for MWNT synthesis, because of a significantly high production rate and high quality tubes with a narrow diameter distribution. Huang *et al.* [64] used TiO_2 support and concluded that Ni is the best catalyst for the growth of aligned CNTs. Therefore, the outcome of the CNT synthesis is a complex *interplay* among the metal precursors, the support, and the reaction conditions.

When the transitional metals are alloyed with another metal, both the carbon yield and the structure of the CNTs can be changed dramatically. This has been demonstrated most extensively by Baker and co-workers with powder catalysts [44, 45, 65]. They have been able to tailor the carbon nanostructures by designing different alloy catalysts. For supported metal catalysts, a similar effect has been observed [66-68]. The ratio of bimetallic catalyst is also important [47, 69]. For CO decomposition on Co-Mo catalysts at 700°C, it was found that a particle with low Co content (<15 at.%) tends to produce a long CNT, while a particle with high Co content (>85%) tends to produce onion-like structure [69].

Even the origin of the metal precursors [70] or the catalyst preparation procedures [71] might play a role. Serp *et al.* [70] found that among iron chloride, iron sulphate, and iron carbonyl, $Fe_3(CO)_{12}$ was the best precursor, producing longest fibers from methane.

2.1.4 Gas precursors

Systematic studies of the relationship between the nature of the carbon-containing gas and the structure of the resulting CNFs are very scarce. The intrinsic activity of the gases will of course determine the CNF growth rate over different catalysts. Hernadi *et al.* [72] observed that over supported iron or cobalt catalysts, the activity of acetylene is higher than that of ethylene and propylene, which are in turn higher than methane. Flame synthesis of CNTs has shown that Fe reacts preferentially with CO/H_2 to produce SWNTs, while Ni reacts preferentially with C_2H_2/H_2 to produce nanofibers [73]. Therefore, the activity of the gases seems to be metal dependent which again illustrates the complex *interplay* between the gases and the metal precursors.

Interestingly, Toebes *et al.* [74] reported opposite reactivity of CNF production from the decomposition of CH_4, CO/H_2, or C_2H_4/H_2 over supported Ni or powder Ni catalyst at 550°C. They found that the small supported Ni particles need gases with a relatively low activity, like CH_4 or CO to produce CNFs. The large unsupported Ni only produces CNFs using C_2H_4. The CNF yield has been attributed to a subtle interplay between the nickel particle size and consequently the exposed crystal planes on the one hand and the reactivity of the gases on the other.

Otsuka *et al.* [75] have shown the effect of the gas precursors on the structure and crystallinity of the CNFs from the decomposition of different hydrocarbons on Ni/SiO_2 catalysts. Zigzag fiber structure was formed from methane, and a rolled fiber structure was formed from alkenes and acetylene. The degree of CNF graphitization was in the order, alkanes > alkenes > acetylene.

2.1.5 Temperature

The temperature appears to influence the CNT yield differently depending on the specific reaction system. Kukovecz *et al.* [76] reported that the amount of CNTs increases with increasing temperature from acetylene decomposition. Takenaka *et al.* [77] found that the CNF yield decreases with increasing temperature from methane decomposition. The CNT yield might also decrease with temperature due to catalyst particle sintering at high temperatures [78].

The effect of temperature on the structures of CNTs has been investigated on Fe/SiO_2 by acetylene decomposition from 600 to 1050°C and gas pressure of 0.6 and 760 Torr. At low gas pressure, the CNTs are completely hollow at low temperature

and bamboo-like at high temperature. While at 760 Torr, all the CNTs are bamboo-like structure regardless of temperature [79]. Therefore, the effect of temperature on carbon structures depends on the gas pressure. Takenaka *et al.* [77] reported fishbone CNFs at 500°C but MWNT at 700°C from methane decomposition on Ni/SiO_2. In addition, the diameter and diameter distribution of the nanotubes will increase with increasing temperature [79-81].

Finally, the reaction temperature influences the graphitic order of CNFs. It has normally been found carbon fibers with more ordered or more disordered carbon after growth at high and low temperatures, respectively [82, 83].

2.1.6 Pressure

Studies of the effect of gas pressure on the production of CNTs and CNFs are less performed. Higher pressures will normally increase the carbon yield but decrease the CNT selectivity [84, 85]. From acetylene decomposition over supported Fe and Co catalyst, Hernadi *et al.* [84] reported that carbon deposit increases with higher pressure, but leads to worse selectivity and many other kinds of carbon structures.

Some studies have observed an optimum partial pressure [86-88]. Liu *et al.* [86] discovered a critical methane partial pressure (~0.4 atm) for SWNT synthesis on supported Fe catalyst. Below this value, the production rate is proportional to the partial pressure. Li *et al.* [88] found that the yields of CNTs increase significantly with the gas pressure from acetylene decomposition over Fe/SiO_2 catalyst, reached 600% at 600 Torr and then decreases with further increase of gas pressure. Li *et al.* [88] also observed a change in the internal structures: completely hollow structure at low pressure but bamboo structure at high pressure.

2.1.7 Hydrogen

The role of hydrogen has been described quite extensively in both the VGCF and CNT literature. Hydrogen is known to either accelerate [78, 89-91] or suppress [80] the formation of CNTs.

The most significant effect of hydrogen is to change the orientation of the graphite sheets [82, 89], which has been illustrated nicely by Jiao and Nolan. Jiao *et al.* [92, 93] found that when no hydrogen was present, only closed forms of carbon deposits such as MWNTs were produced from CO. As the hydrogen partial pressures increased to 0.1 vol%, the filament with open edges was observed. The number of open edges and the angle between the graphite sheets and the axis increased with increasing H_2 concentration. Nolan *et al.* [94] found that carbon deposition from CO resulted in encapsulated carbon only when hydrogen was absent. Nolan *et al.* [95] proposed that hydrogen atoms serve to satisfy valences at the free edges of graphite sheets. Without hydrogen, carbon will deposit in closed forms such as shells and nanotubes. Equations were derived to calculate the minimum number of hydrogen atoms necessary to form a CNF. Nolan *et al.* [96] further derived thermodynamic expressions for the relationship between filament cone angle and hydrogen partial pressure. Therefore, the orientation of graphite basal planes of carbon filaments can be tailored.

2.1.8 Particle size

Though it is widely accepted that the final CNT diameter is determined by the starting catalyst particle size, the relationship between tube diameters and sizes of

initial catalyst particles can be complicated by particle mobility, sintering and redispersion. Catalyst particles could either be aggregated by contact with the reactant [97], or be changed by the deposited carbon [98]. Kukovitsky *et al.* [99] investigated more systematically the dependence of CNT diameter on the size of the Ni catalyst: At low temperature of 700°C, the nanotube growth is conducted through the solid tip catalyst and the tube diameter reproduces essential features of original particle size distribution. At 800°C, it grows via liquid catalyst particle by extrusion mode and tubes exhibit universal Gauss-like distribution irrespective of the catalyst particle sizes.

Recently it has been noticed that the catalyst particle size is an important factor in CNT growth rate [77, 100, 101]. Indeed, it has been shown decades ago both experimentally and theoretically that the carbon filament growth rate increases with decreasing catalyst particle size [102, 103]. Some recent studies showed that the CNT growth rate and productivity are higher on the larger particles [104], while others found that the growth rate is higher on smaller particles [54]. This suggests that there is probably an optimum particle size for CNT growth, which has been implicitly demonstrated [85, 105, 106]. Peigney *et al.* [85] examined the decomposition of CH_4/H_2 on α-$Al_{1.9}Fe_{0.1}O_3$ solid solution. Almost all the CNTs have an inner diameter in the range of 1-6 nm, indicating that the catalyst particles active for CNT formation are in this size range. Another study showed that the hematite particles with a 8-20 nm size range are involved in the formation of MWNTs during C_2H_2 decomposition at 700°C [105].

In addition to the above discussed parameters, other factors such as run duration [78, 107] , phosphorus [108], and sulfur [109, 110] *etc.* have been found to influence the CNF and CNT growth. Therefore, the growth of CNTs is a very complex process which involves the *interplay* of all the process parameters.

2.1.9 SWNT

The synthesis of SWNT needs additional notice. The lack of methods for large scale synthesis has limited fundamental research and application development of this unique material. A yield of 550% relative to the weight of metal [111], or 120% to 200% [112, 113] relative to the catalyst weight has been claimed as very high.

It is very important that the metal particles are not aggregated during the SWNT growth process [107, 114]. Li *et al.* [115] demonstrated an upper limit size of 8.5 nm to nucleate SWNT over Fe-Mo catalysts dispersed on Al_2O_3 film. Particle aggregation could be prevented by providing a nucleating agent such as Mo, Ru, and W, in addition to catalyst precursors, which would rapidly adsorb the precursor atoms (Fe, Co, Ni) [114]. Therefore, the catalysts consist of Fe-Mo [116-118] or Co-Mo [119-122] bimetallic species have been very frequently used. Other special catalyst precursors have also been studied, for example ferritin [123-125], nickel formate [126], or ferrocene [127].

Mo provides a synergistic effect to Fe in SWNT synthesis [128]. The interaction mechanism was studied by Hu *et al.* [129], and has been systematically investigated by Alvarez *et al.* [120-122]. It was concluded that the catalysts are effective when both metals are simultaneously present. When they are separated they are either inactive (Mo alone) or unselective (Co alone). The selectivity of the Co-Mo catalysts toward SWNTs depends on the stabilization of Co species in a nonmetallic state before exposure to the carbon containing gases [130]. If Co-Mo interaction is

disrupted, SWNT selectivity decreases sharply [131]. The Co-W synergism has been disclosed accordingly [132].

With respect to the catalyst support, MgO seems to be the preferable support for SWNT growth [133]. MgO is easier to be removed and provides higher yield with a smaller diameter compared with for example Al_2O_3 [134]. The gas sources used in the synthesis of SWNT are mostly methane, though CO, ethylene or acetylene have been frequently used.

The most successful process up to now is the HiP_{CO} process [114, 135], in which the production of SWNTs is induced by the decomposition of $Fe(CO)_5$ in flowing CO at high pressure and elevated temperature. Iijima *et al.* [136] very recently reported a breakthrough in the synthesis of SWNTs. By adding water to the standard SWNT synthesis scheme, the yields reached astonishingly 50000% relative to the starting metal. The results are so remarkable, suggesting that large scale synthesis of SWNTs is no longer a dream.

2.2 Growth mechanism

The mechanism of the catalytic growth of CNFs has been studied and debated for a long time [17, 19, 137]. It is now commonly accepted that the growth of a carbon filament proceeds through three steps, which can be represented by a simplified model as in Figure 2.1. The first step is the decomposition of carbon-containing gases on the metal surface at the gas-particle interface. The second step involves carbon dissolution in the particles, and carbon diffusion through the bulk or on the surface of the metal particles. In the final step, carbon precipitates on the form of CNFs or CNTs at the other side of the particle.

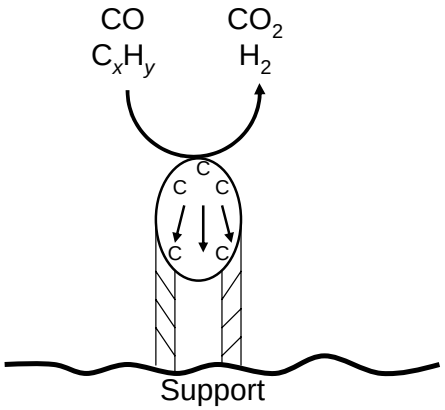

Figure 2.1. *A simplified model of the CNF/CNT growth process.*

This mechanism works well at least for the formation of CNFs and MWNTs. In most cases, the rate determining step is the diffusion of carbon through the catalyst particle. Justification for this claim is based on the remarkable agreement between the measured activation energies for filament growth and those for carbon diffusion [17, 20, 137, 138]. B.Nagy *et al.* [138] compared the activation energy for nanotube growth measured by *in situ* electron microscopy and the activation energy for carbon diffusion on Ni, α-Fe, γ-iron, Ni-Fe, Co, V, Mo, Cr, the values are always strikingly similar. Resasco *et al.* [139] also concluded that in the SWNT synthesis once the nucleation is completed, the formation rate is controlled by mass transfer.

In certain cases the rate-limiting step can be reversed. For example, for CNF formation from acetylene decomposition on α-Fe, the diffusion of carbon is the rate-limiting step. However, when CNF grows from a number of more stable hydrocarbons, the carbon diffusion is not rate limiting but rather the surface reactions [20].

The similarity between the activation energies of filament growth and carbon diffusion suggests that carbon diffuses through the bulk of the metal. However, Helveg *et al.* [140] believe that only surface carbon diffusion has taken place. They directly imaged the CNF growth process using *in situ* high resolution transmission electron microscope. It was observed that Ni step edges play a key role and that the process involves the transport of C atoms towards and Ni atoms away from the graphene-Ni interface. This observation is also consistent with a molecular dynamics study [141]. Then probably both surface and bulk diffusion take place, depending on the reaction conditions.

The details of the nucleation of both SWNTs and MWNTs have been formulated by Dai *et al.* [142] through the so-called *yarmulke* mechanism. They proposed that a graphene cap will be assembled on the particle surface, with its edges strongly chemisorbed to the metal. Newly arrived carbon will continue to assemble on the surface of the catalytic particle, and will go to three possible sites: (1) The original surface shell can continue to grow, which would result in overcoating and deactivation of the catalytic particle. (2) A second cap can form underneath the first, spaced by roughly the interlayer spacing of graphite. Then old caps are forced to lift up by forming cylindrical tubes whose open end remains chemisorbed to the catalytic particle. (3) Carbon can add to the cylindrical section of a growing layer. B.Nagy *et al.* [138] depicted a more explicit picture of how such a cap forms for SWNTs (Figure 2.2): the supersaturation leads to the segregation of the carbon atoms, which move to the surface and combine to form an initial graphene or haeckelite layer. After reaching a critical size and if the system contains enough kinetic energy, it may detach from the particle surface and form a fullerene-like cap. This early stage of carbon nucleation on the metal surface is probably common for both MWNTs and SWNTs.

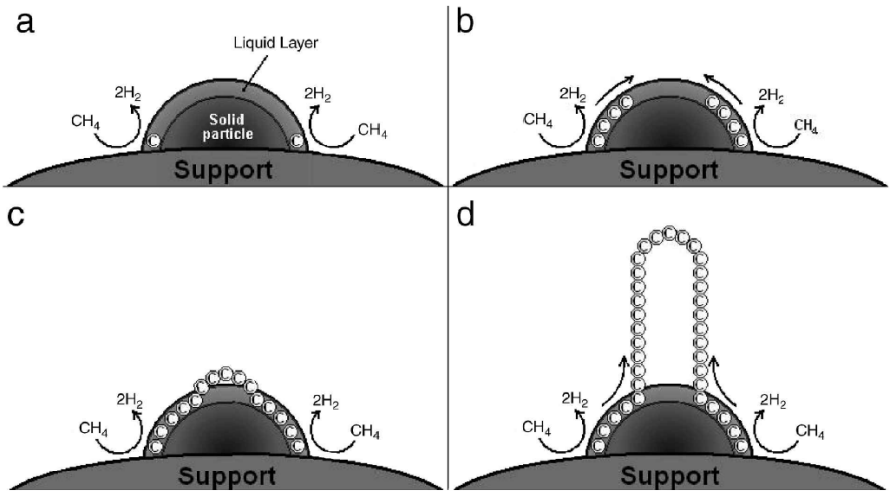

Figure 2.2. *Schematic view of the nucleation of a cap and a SWNT. (a) Hydrocarbon decomposition. (b) Carbon diffusion in the surface layer. (c) Supersaturation of the surface and formation of the cap. (d) Growth of a SWNT (from B.Nagy et al. [138]).*

The nucleation of a fishbone or platelet nanofiber would differ from that of a parallel tube. For the fishbone or platelet structure, each layer is probably segregated

separately due to supersaturation. There is no continuity in the flux of carbon atoms through the particle surface to the fiber. One of the prerequisite for the formation of fishbone/platelet fibers is hydrogen being abundantly present on specific surface planes of the catalyst particle. Hydrogen saturates the dangling bonds at the edges, and probably also initiates the segregation of graphite layers. This leads each graphite layer to nucleate separately [143].

During the CVD growth, the metal particles are possibly in the molten state [144, 145]，which has been always assumed in high temperature process such as laser vaporization [146-149]. This is because the carbon saturated metallic nanoparticles melts at temperatures far below the bulk melting point of the metal [144]. B.Nagy *et al.* [138] proposed only a liquid surface layer for SWNT growth.

The last question is why different carbon nanostructures occur. The carbon deposit structure seems to depend in a complex manner on the reaction conditions, gas precursors, and the metal catalysts. For example, large particles are not able to grow SWNTs, but known to grow MWNTs and nanofibers [139, 150]. Too large metal particles tends to form encapsulating carbon instead of carbon filaments [142, 151]. The use of metals characterized by a higher metal carbon energy bond yields nanotubes with smaller diameters [145].

Snoeck *et al.* [152] have provided an elegant kinetic model explaining why full or hollow fibers are formed from supported metal particles. This model shows that CNFs tend to form at low temperatures and tubular structures tend to form at higher temperatures. The carbon deposit structure is also affected by thermodynamic factors. Carbon deposits will have their basal planes predominantly parallel to the planes of the catalytic particles. This occurs because the interfacial free energies between the particles and the carbon deposits is smaller [153]. Therefore, the morphology of the carbon deposit is also determined by the surface orientation of the particles, which in turn is influenced by the reaction conditions.

It is not clear whether or not exactly one mechanism accounts for the growth of all CNTs. *In situ* thermal analysis-mass spectroscopic study of CNT growth surprisingly detects no hydrocarbon species decomposed from benzene over Fe-Co/γ-Al_2O_3 at 700°C, indicating that C-C bonds were never broken during CNT growth [154].

2.3 Application in hydrogen storage

The first report on hydrogen storage in SWNTs estimated a high storage capacity of 5-10 wt.% [155]. In 1998 an extremely large hydrogen uptake of 67 wt.% was announced by Baker & Rodriguez [156]. Later, Liu *et al.* [157] reported a capacity of 4.2% for SWNTs and Chen *et al*. [158] reported up to 20% in Li doped CNFs. Researches on hydrogen storage in carbon nanostructures have exploded since then, and numerous reviews can be found [159-167].

It should be noted that nearly all results are not confirmed or reproduced by other independent groups, and has been doubted ever since. The hydrogen uptake in the alkali-doped CNT of Chen *et al.* [158] has been shown to be due to the contamination of water [168, 169]. Hirscher *et al.* [170, 171] demonstrated that the contamination of carbon materials with metals have lead to the majority of uptake in SWNTs. Later more studies have claimed that the high storage capacities in carbon nanostructures are unjustified and are indeed very low [161, 172-174]. The literature is full of debate, and this “hydrogen storage controversy” was highlighted by an article in *Nature* [175]. Despite all these controversies, there are still new results attracting the interests of researchers and energy and car companies.

Most of the hydrogen adsorption experiments have been carried out with volumetric [156, 176] and gravimetric methods [157, 168, 169], or temperature programmed desorption spectroscopy [165]. Each method can easily bring erroneous results if the system is not carefully designed and calibrated. For good accuracy of the volumetric method, it typically requires specimen masses of 500 mg or higher. Any leakage or ambient room temperature variations may give rise to large experimental errors [174]. For the gravimetric method, upon a change in temperature or gas flowrate, the accompanying change caused by changes in buoyancy and friction forces from the gas flow can be usually of the same order of magnitude as the signal that is being measured [168].

The storage capacity at room temperature has been demonstrated to be correlated with the BET specific surface area [160, 177-179]. This suggests that physisorption is responsible for the hydrogen uptake. However, Browning *et al.* [180] observed substantial levels of hydrogen uptake up to 6.5 wt.% under conditions of 12 MPa pressure and ambient temperature, which can not be interpreted by physisorption alone and a slow chemisorption process has been suggested. Orimo *et al.* [160] proposed the defect mediated hydrogen sorption, which is an intermediate state between physisorption and chemisorption. They believe that the formation of defective structures is critical for producing the nonphysisorbed hydrogen. This is manifested by Lueking *et al.* [181], who found that the generation of structural defects is essential for hydrogen storage.

More recent research efforts have concentrated on the carbon-metal composite materials [182, 183]. Callejas *et al.* [184] observed an increase of 40% in hydrogen adsorption when the SWNTs are reduced. The reduction process will lead to hydrogen dissociation by the reduced metal nanoparticles with subsequent hydrogen spillover and chemisorption. The metal can also increase the adsorption rate [185] and reduce the desorption temperature [186].

Careful *in situ* pretreatment of CNF samples is a critical procedure in order to reach high adsorption capacity [165, 187-189]. It will remove chemisorbed gases from edge regions [187]. In metal doped CNTs, the increase in pretreatment temperature also likely enhances the metal-support contact for higher hydrogen uptake [189].

Ning *et al.* [190] have for the first time used large quantities of MWNTs up to 85 g for hydrogen storage by a volumetric flow meter. It was claimed that a precision of 0.01% can be obtained. At a pressure of 12 MPa, the hydrogen uptake by pretreated MWNTs at room temperature was no more than 0.30 wt.%, though reached 2.27 wt.% at 77 K.

3 EXPERIMENTAL

3.1 Catalyst preparation

The catalysts used in paper 1, 2, and 3 are hydrotalcite (HT) derived Ni-Fe/Al_2O_3 catalysts, which have high metal loadings. The catalysts used in paper 4 are Ni-Fe/Al_2O_3 supported catalysts prepared by homogeneous deposition-precipitation from cyanide precursors. The catalysts used in paper 5 and 6 are prepared by homogeneous deposition-precipitation using different precipitation agents, impregnation, or sol-gel methods to obtain varying particle sizes. The catalysts used in paper 7 are a Fe powder catalyst with small particle size and a Fe/Al_2O_3 catalyst derived from HT. In all cases, a small particle size and narrow size distribution have normally been the purposes. The detailed preparation procedures are given in the respective papers with references to relevant literature.

3.2 CNF/CNT synthesis

The CNF/CNT synthesis apparatus is presented in Figure 3.1. The synthesis was performed in a vertical quartz flow reactor with 4 cm diameter and 50 cm length. A quartz sinter is located in the middle of the reactor upon which the catalysts can be loaded. In each synthesis, a weighted amount of catalyst samples were reduced in 100 ml/min He/H_2 mixture (50% vol) at 600°C overnight. The temperature was raised to 600°C at 5°C/min. Following reduction the system was flushed for 0.5 h with helium. The reactor was then raised to the synthesis temperature, and a desired mixture of carbon-containing gases was introduced into the reactor. The composition of the gaseous products out of the reactor was analyzed by an online gas chromatograph (HP 5890). The carbon selectivity, CNF growth rate, and CNF productivity can be calculated from GC analyzed results. The total amount of CNFs produced on the catalysts during time on stream was also determined gravimetrically after the system had been cooled down to ambient temperature under flowing helium. In most cases the gravimetrically determined CNF amount was very close to the GC calculated result.

3.3 Catalyst and CNF/CNT characterization

3.3.1 XRD study

X-ray diffraction (XRD) study was carried out for both the catalysts and CNF samples. For phase identification, a Simens D5005 X-ray diffractometer was used. Diffraction was performed with Cu K_α radiation and peaks were identified by comparison with standards in a database. For determining particle size distribution of the catalysts, a Siemens D5000 X-ray diffractometer was used with Cu $K_{\alpha 1}$ radiation. The resulting peaks were analyzed with a profile fitting program (SIEMENS DIFFRAC^{plus} PROFILE), and crystal size and microstrain software (DIFFRAC^{plus} WIN-CRYSIZE). For characterization of the reduced catalyst sample, the catalysts were pre-reduced and passivated to prevent bulk oxidation of the catalysts.

XRD study of CNFs was performed with the Simens D5005 X-ray diffractometer. Comparing the d_{002} values with the theoretical value of graphite, 0.33542 nm, provides an indication of the degree of graphitic character [191, 192].

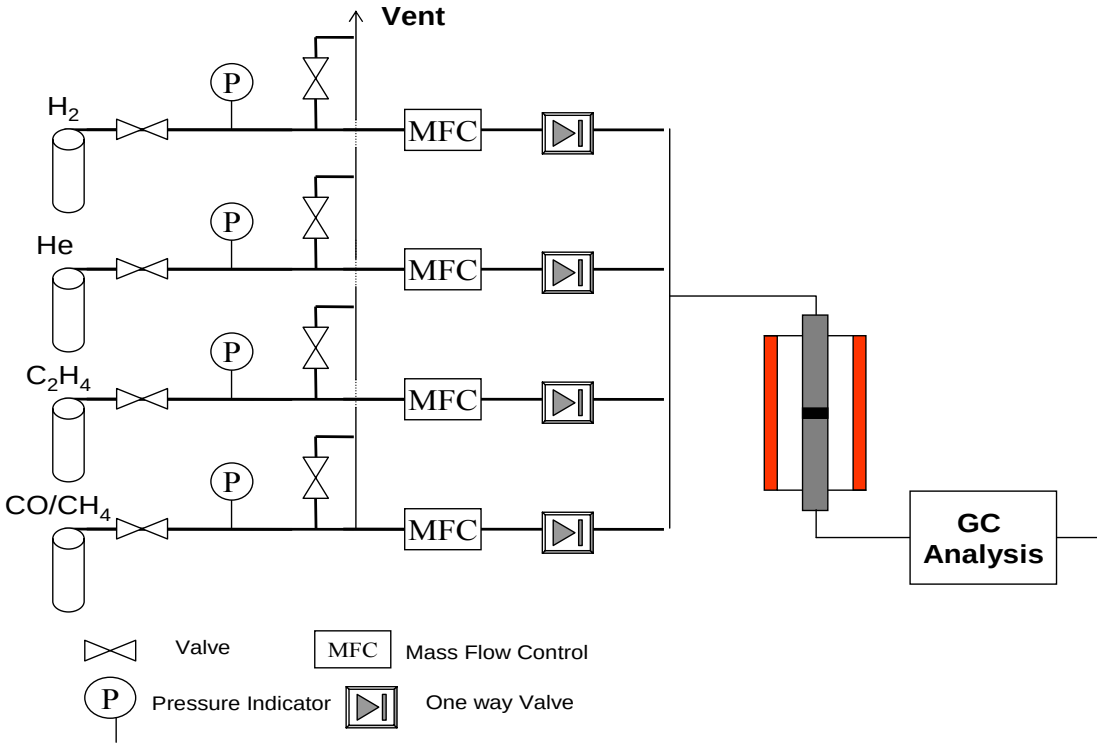

Figure 3.1. *The CNF/CNT synthesis apparatus.*

3.3.2 Thermogravimetric analysis (TGA)

Simultaneous thermogravimetry (TG) and differential thermal analyses (DTA) were carried out both for the HT precursors and CNFs, using a Perkin-Elmer thermogravimetric analyzer (TGA) apparatus. TGA study of the HT catalysts was carried out in 40 ml/min air at a heating rate of 10°C/min from 30°C to 800°C using 11-14 mg samples.

TGA study of CNFs was performed in 80 ml/min air at a heating rate of 10°C/min from 30°C to 900°C using 8-9 mg purified samples. The TGA method provides a convenient means of characterizing the stability of CNFs towards high temperature oxidation and of assaying the degree of graphitization [193]. The rates of interaction with gases are slowest within a basal plane surface and fastest at defects (vacancies, dislocations, and steps) and at the termination of basal planes (*i.e.*, dangling bonds at edges) [194, 195].

3.3.3 TPR study

Temperature programmed reduction (TPR) is a highly sensitive method for discriminating the reducibility of different species, providing information about its chemical state, as well as its dispersion state. TPR study was carried out in a CHEMBET-3000 TPD/TPR instrument. TPR was performed in 80 ml/min H_2/Ar mixture (7% vol H_2) at a heating rate of 10°C/min from 30°C to 1000°C using about 35 mg samples.

3.3.4 Chemisorption

The measurement of the adsorption capacity of supported metals is useful in providing estimates of metal surface, dispersion, and average crystallite diameter. Hydrogen chemisorption was performed with a Micromeritics ASAP 2000 apparatus with about 0.3 g pre-reduced catalyst samples at 35°C.

3.3.5 BET study

The BET study was carried out for both the catalysts and the CNF samples. The measurement used a Micromeritics TRiStar 3000 apparatus and about 0.12 g samples by nitrogen adsorption. Before collecting the BET isotherms the samples had been evacuated to 50 mTorr at 300°C.

3.3.6 SEM study

The characteristics of the carbon deposits were examined using scanning electron microscopy (SEM). The SEM study was performed with a Hitachi S4300 field emission electron microscope. The samples were prepared by dropping some CNF powders onto a wet carbon tape, and then dry the sample at 80°C overnight. The pictures were taken with a secondary electron detector.

3.3.7 TEM study

The transmission electron microscopy (TEM) investigation was performed for both the catalysts and the CNFs, using a JEOL 2010F electron microscope equipped with a field emission gun. TEM specimens were prepared by ultrasonic dispersion of the CNFs or catalyst samples in ethanol, and then a drop of the suspension was applied to a holey carbon support grid.

3.4 Hydrogen storage apparatus

The hydrogen storage apparatus is displayed in Figure 3.2. It consists of a sample cell connected to a hydrogen reservoir via a high-pressure mass flow controller (MFC), which can endure pressures up to 120 bar. The sample cell can be heated to 1000 °C inside an electric oven. Thus the samples can be pretreated *in situ* at high temperatures. The sample cell is also connected to a vacuum pump for degassing. The system pressure is measured with a high-pressure transducer. All the parameters, including temperature, pressure, gas flow rate, and flow time are controlled and recorded by a Labview program with the computer.

For each adsorption-desorption cycle, the hydrogen uptake amount can be calculated from the flow rate, flow time, and pressure. The desorbed hydrogen will also go through the MFC and is measured in a similar way. Subsequently the adsorption-desorption isotherm can be constructed.

Another feature of the setup is that it has been designed to measure the storage capacity with tens of grams sample quantity. Traditionally the hydrogen adsorption measurements are performed with sample amounts of only several or tens of milligrams. Very easily, parasitic effects may be ascribed to hydrogen uptake. With large amount of sample masses, the artificial results are minimized effectively.

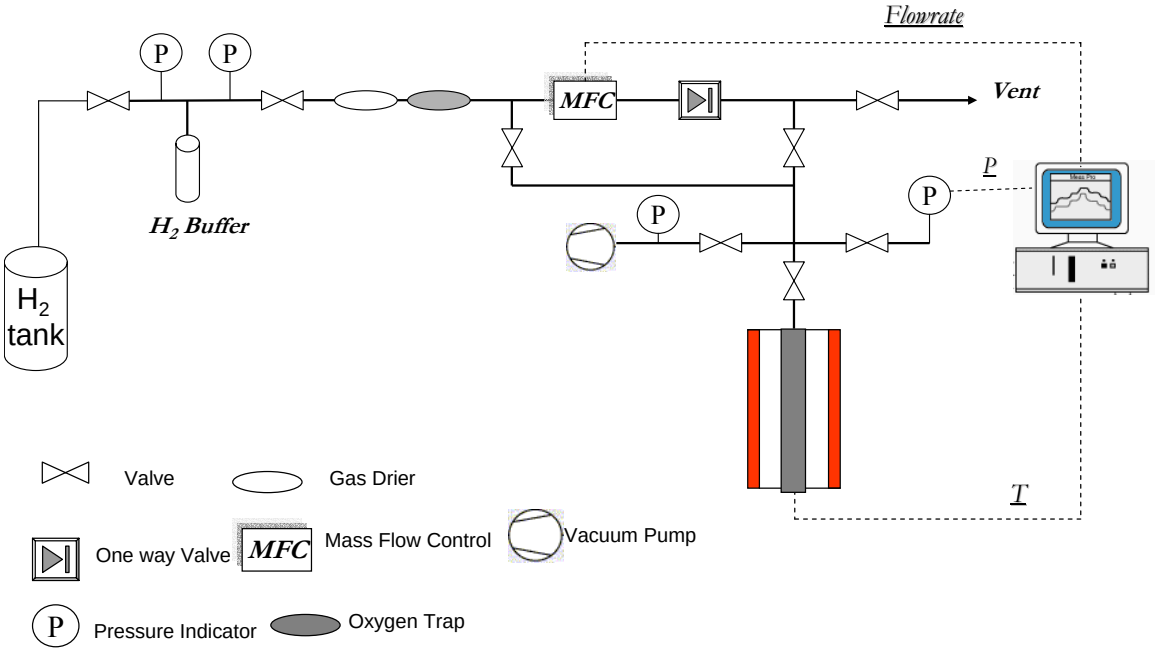

Figure 3.2. *The hydrogen storage apparatus.*

4 RESULTS AND DISCUSSION

4.1 CNF synthesis on hydrotalcite derived catalysts (Paper 1, 2, and 3)

HT derived catalysts will result in a highly dispersed mixture of the cations on an atomic scale, with desirable properties such as high surface area, high thermal stability, and high metal loadings. This will facilitate the growth of CNF with high productivity and quality simultaneously.

Paper 1 presents a detailed study of the preparation and characterization of the HT derived Ni-Fe/Al_2O_3 bimetallic catalysts, with Ni/Fe ratios of 1:0, 8:2, 5:5, 2:8, and 0:1. The structure and properties of the catalysts were carefully examined by various methods such as XRD, TGA, TPR, BET, chemisorption, XPS, and EXAFS. It turns out that pure HT structure can only be synthesized at low Fe^{2+} concentration and that the percentage of the impure structure (spinel) increases with the increase of Fe^{2+} ratio. The formation of spinel phase instead of pure HTs from Fe^{2+} can be attributed to the large ionic radius of Fe^{2+}, and the easy oxidation of Fe^{2+} to Fe^{3+}. It is then difficult to incorporate all the Fe^{2+} ions into the HT structure, and the excessive Fe was separated out as Fe_3O_4 or $NiFe_2O_4$ spinels. Pure HT structure derived Ni-Fe catalysts have small particle sizes and narrow particle size distribution, in spite of a high metal loading of 77 wt.%. If impure spinel phase is formed, the particle size distribution increases significantly. The HT derived catalysts also have high surface areas, which decrease if the spinel phase is formed. Therefore it is essential to prepare pure HT structures.

The phases of different catalysts after reduction are shown in Figure 4.1. It is clear that for the NiFe (5:5) and NiFe (2:8) catalysts, two different alloy phases are present. XPS and H_2 chemisorption studies found that Fe is enriched on the alloy catalyst surfaces after reduction.

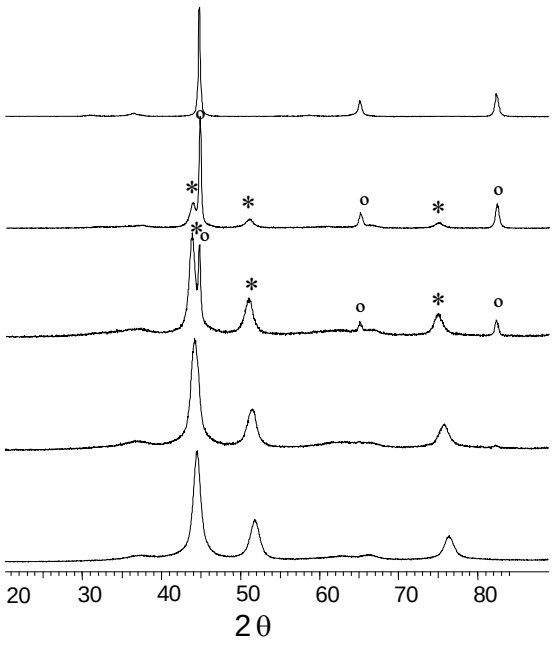

Figure 4.1. *XRD patterns of the reduced catalysts. From bottom: Ni, NiFe (8:2), NiFe (5:5), NiFe (2:8), Fe. Peaks marked with * and o are characteristic of two different Ni-Fe alloy phases. For clarity when single phase is present, the peaks are not marked.*

Paper 2 presents the synthesis of CNFs from CO disproportionation and C_2H_4 decomposition on the HT derived Ni-Fe/Al_2O_3 catalysts. It was found that only Fe catalyst is able to produce CNFs from CO disproportionation, whereas other catalysts will deactivate very fast in CO. Only Ni catalyst can produce CNFs from C_2H_4 decomposition, whereas other catalysts will produce tar instead of CNFs. However, when C_2H_4/CO mixtures are the reactant, all catalysts are able to produce large amount of CNFs from C_2H_4 decomposition. Figure 4.2 shows that all the catalysts have very high productivity, which slightly decreases with the increase of Fe concentration. GC analysis shows that CO is not converted in the reaction mixture and that the concentration of CO has no real influence on either C_2H_4 conversion or the carbon selectivity.

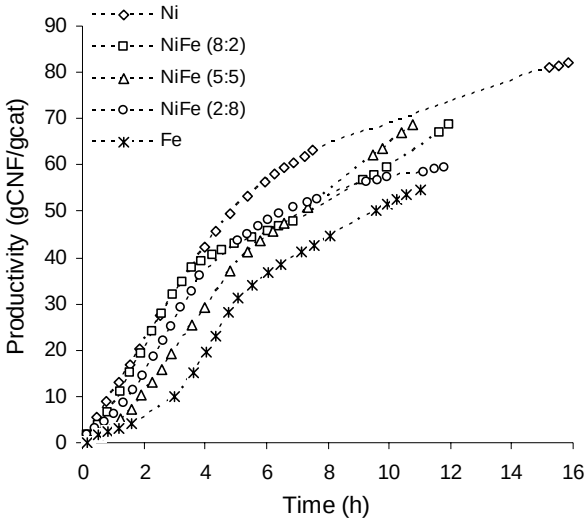

Figure 4.2. *CNF production as a function of reaction time over various Ni-Fe catalysts from C_2H_4/CO/H_2 (30:10:10) at 600℃.*

The Ni-Fe bimetallic surfaces are enriched with Fe, which are not preferred for C_2H_4 decomposition. In contrast, in the presence of CO, the surfaces may reconstruct to have a set of crystallographic faces, and/or Ni segregation, that are favored for C_2H_4 decomposition, but suppresses CO dissociation. CO may also play an electronic effect by electron withdrawing that promotes the C=C bond rupture. These two effects made all catalysts active in producing CNFs from the mixture of C_2H_4 and CO.

SEM, TEM, TPO, and XRD characterization shows that CNFs with different crystalline nature and morphologies were produced from different catalyst composition and gas precursors. SEM and TEM studies confirmed that the structures are always relatively uniform and that the method used for the synthesis of CNFs was selective, since very little other forms of carbon were observed. This is represented by a SEM image of CNFs produced over the NiFe (5:5) catalyst from C_2H_4/CO/H_2 (30:10:10) at 600°C (Figure 4.3). The synthesized CNFs normally have diameters ranging from 5 to 80 nm. The average diameters vary from 19 to 55 nm.

Therefore, more control over the final structure and diameter of the CNFs is achieved with the HT catalysts, a condition normally realized with supported catalysts. Moreover, a high yield is obtained with the HT catalysts, which is superior to the supported catalysts. In conclusion, it is demonstrated that using HT derived Ni-Fe/Al_2O_3 presents a new promising route for large-scale controlled synthesis of CNFs.

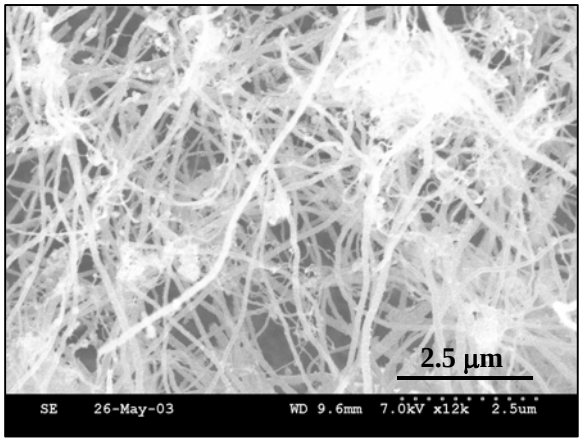

Figure 4.3. *SEM image of CNFs produced from C_2H_4 decomposition with $C_2H_4/CO/H_2$ (30:10:10) on the NiFe (5:5) catalyst at 600℃.*

Paper 3 is a further study to optimize the large scale CNF synthesis processes from $C_2H_4/CO/H_2$ (30:10:10) on the HT derived catalysts. From paper 2 it was found that a high Ni ratio is preferred for ethylene decomposition, therefore a new catalyst of NiFe (6:1) was prepared, in addition to the NiFe (5:5) catalyst from paper 2. The synthesis has been optimized as a function of various parameters such as hydrogen content, gas space velocity, and temperature.

The effect of these process parameters on the outcome of the CNFs is represented in Table 4.1. It was clear that high hydrogen concentration, space velocity, and reaction temperature will enhance the production of CNFs. However, a slightly lower quality is always associated with a higher productivity. For example, the increase of the reaction temperature significantly increased the productivity and crystallinity, but produced CNFs with very large diameter and much shorter length. The increase of the hydrogen concentration increased the CNF productivity at the expense of a large diameter. Therefore, for practical applications, there is a compromise to be made. Moreover, the highest productivity has reached 128 gCNF/gcat during 8 h on the NiFe (6:1) catalyst with good quality.

Table 4.1. *Influence of catalysts and process parameters on the CNF productivity, production rate, and properties.*

Ni:Fe	C_2H_4:CO:H_2/ T (°C)	gC/gcat [a]	Rate (gC/gcat *h) [b]	Mean diameter (nm)	Max. weight loss T (°C)	d_{002} (Å)
6:1	30:10:5 /600	76.2 (8.3)	9.36	ND[c]	585	3.454
6:1	30:10:10/600	100.9 (13.8)	9.98	42	608	3.447
6:1	30:10:15/600	103.8 (12.0)	10.33	53	611	3.434
6:1	60:10:10/600	127.8 (8.2)	15.80	47	632	3.461
5:5	30:10:10/550	29.9 (8.3)	3.73	ND	564	3.469
5:5	30:10:10/600	63.6 (9.8)	6.90	37	611	3.437
5:5	30:10:10/650	64.3 (8.1)	7.94	70	634	3.426

[a] Different synthesis time was used (values in the parenthesis); [b] For comparison the rates under different conditions were calculated based on 8 h synthesis time; [c] Not determined.

4.2 CNT synthesis on supported catalysts (Paper 4)

Paper 4 presents CNT synthesis over the supported Ni-Fe/Al_2O_3 catalysts with 20 wt.% and 40 wt.% metal loading from CO disproportionation. The parameters of

space velocity, loading, hydrogen, and temperature on CNT production rate, productivity, and morphology has been studied.

Table 4.2 shows that a high space velocity will result in a high production rate but a short lifetime and a low carbon capacity. Therefore, there is a comprise to be made. Increasing the metal loading to 40 wt.% significantly increases the production rate and productivity. The effects of space velocity and metal loading on the catalyst lifetime and carbon capacity can both be interpreted by the CO_2 effect, which acts as gasification agent to prevent encapsulating carbon formation.

Table 4.2. *Catalyst activity at different metal loadings and space velocities.*

Catalysts	Space velocity (l/gcat*h)	Lifetime (h)	Carbon capacity (gC/gcat)	gC/g metal	Average growth rate (gC/gcat*h)
Ni-Fe (20)	9.6	74.1	41.9	209.4	0.56
Ni-Fe (20)	19.2	24.3	15.7	78.3	0.64
Ni-Fe (40)	19.2	55.6	101.3	253.3	1.82

TEM images show that the CNTs produced over these supported catalysts have very homogeneous structure and diameters (Figures 4.4 (a) and (b)). At the high metal loading and space velocity, the CNTs are as uniform as those at the low metal loading but the CNTs are highly entangled (Figure 4.4 (b)).

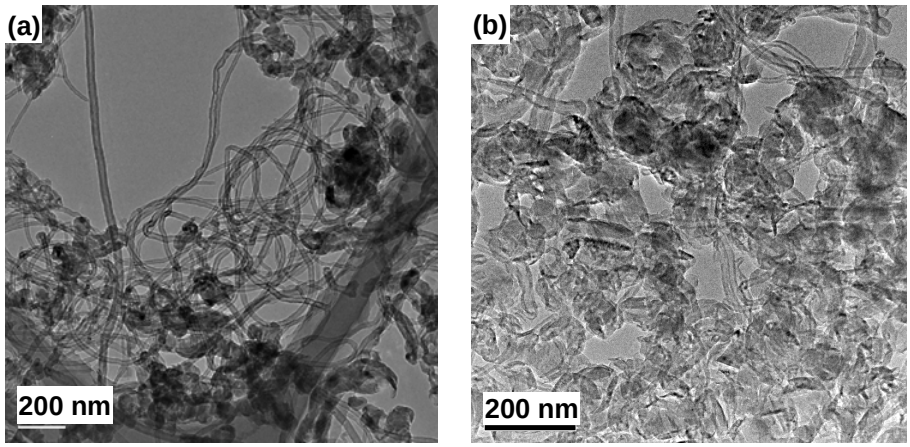

Figure 4.4. *Low resolution TEM images of (a) CNTs produced from CO/H_2 (40/10) at 600℃ on the Ni-Fe (20) catalyst; (b) CNTs from CO/H_2 (80/20) at 600℃ on the Ni-Fe (40) catalyst.*

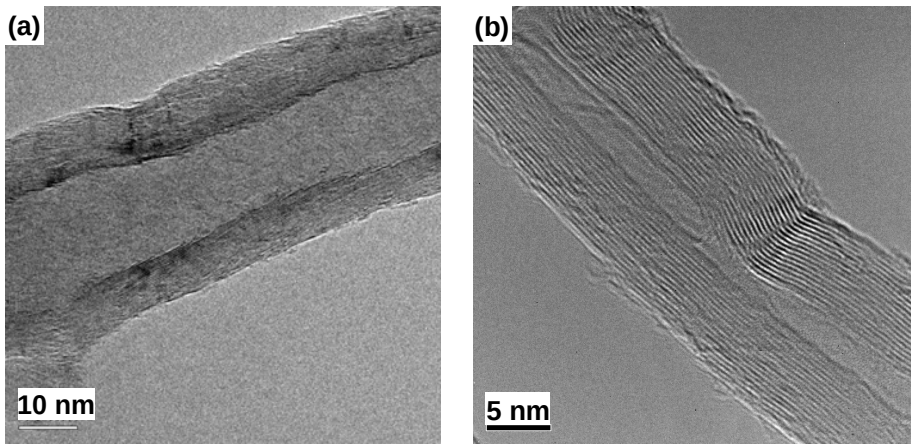

Figure 4.5. *HRTEM images of CNTs produced on the Ni-Fe (20) catalyst at 600℃ (a) graphite sheets inclined at an angle to the tube axis from CO/H_2 (40/10); (b) walls with no open edges from CO (40).*

H_2 is necessary for a high productivity, since without H_2 the catalyst deactivates very fast. The partial pressure of H_2 can be utilized to adjust the CNT nanostructure. Figure 4.5 (a) shows that in the presence of H_2 the walls of the CNTs are oriented at a small angle with respect to the tube axis, whereas the CNTs produced without H_2 shows no open edges (Figure 4.5 (b)).

Finally, low temperature results in a high initial production rate but again a short lifetime and a low carbon productivity. CNFs with relatively poor crystallinity are produced at the low temperature.

4.3 Mechanistic study of CNT growth (Paper 5, 6)

Paper 5 and 6 presents our understanding of increasing CNT production rate and productivity from a mechanistic point of view. In paper 5, a series of silica supported Fe catalysts were prepared by different methods in order to obtain varying Fe particle sizes. The catalyst particle sizes were studied by XRD and TEM. The CNT growth from CO disproportionation was studied in order to establish a relationship between the CNT growth rate and the particle size. It is found that there is an optimum catalyst particle size at around 13-15 nm which will lead to the maximum growth rate. This has been demonstrated at two different synthesis temperatures of 600 and 650°C. The correlation is shown in Figure 4.6.

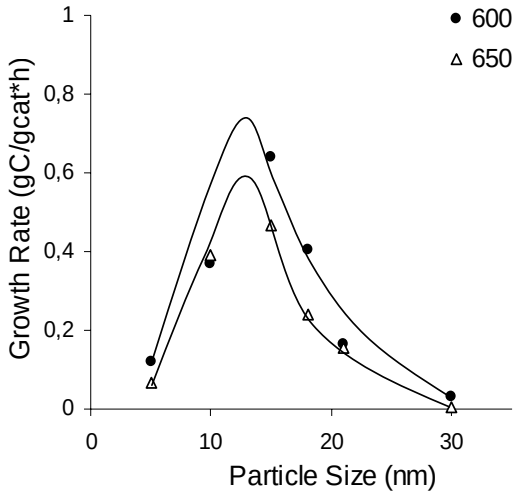

Figure 4.6. *Dependence of growth rate on the particle sizes at 600 and 650℃.*

The size effect can be explained by a mathematical model. At steady state, the filament growth rate is directly proportional to the driving force of the carbon diffusion, which can be simplified as:

$$r = \frac{D_C}{d_{Fe}} a_{Fe} (C_{C-Fe,f} - C_{C-Fe,r})$$

where r is CNT growth rate, D_c is effective carbon diffusivity, a_{Fe} is specific surface area of Fe, d_{Fe} is effective diffusion length, $C_{C\text{-}Fe,f}$ is carbon concentration at the gas side, and is in equilibrium with surface carbon. $C_{C\text{-}Fe,r}$ is carbon concentration at the rear side of the catalyst particle, and is identical with the saturation concentration of CNT (C_{sat}). Therefore, a small crystal size of Fe will provide a large surface area for the surface reactions, a high diffusion flux area and a shorter diffusion length, which is beneficial for a high growth rate. On the other hand, a small crystal

size will result in a large saturation concentration of CNT, leading to a low driving force of carbon diffusion, and a lower growth rate. The net effect of the Fe particle size on the rate of CNT formation is a result of the competition among all the factors and will lead to an optimum size with the fastest rate.

Numerous studies have shown that catalyst support will influence the CNT growth rate. In paper 6, the dominating factor between the particle size and catalyst support that determines the CNT growth rate is demonstrated. The CNT growth was also studied from CO disproportionation over Fe catalysts supported on SiO_2 and Al_2O_3. The following four catalysts Fe/SiO_2 (UREA), Fe/Al_2O_3 (UREA), Fe/SiO_2 (CYA), and Fe/Al_2O_3 (CYA) have sizes of 11.6, 28.9, 30.2, and 38.5 nm, respectively. From Figure 4.7 it is clear that the Fe/SiO_2 (UREA) catalyst with the smallest particle size has a much higher growth rate than the others. The Fe/Al_2O_3 (UREA) and Fe/SiO_2 (CYA) catalysts have similar particle sizes, and the growth rates are different but the difference is not so significant. This trend is demonstrated also at two different temperatures of 600 and 650°C. Consequently it can be concluded that the particle size is determining the CNT growth rate.

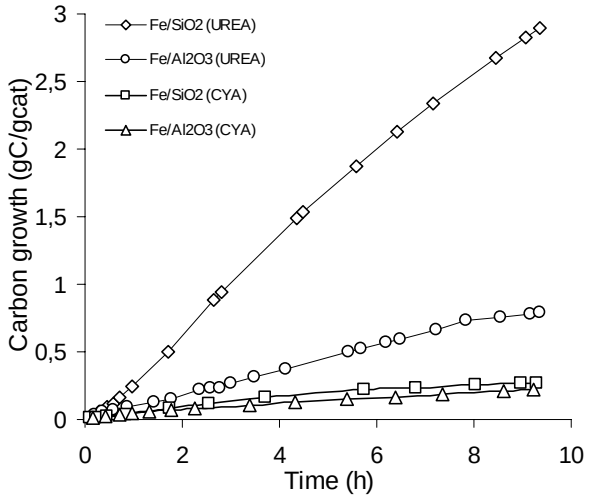

Figure 4.7. *CNT growth over different Fe catalysts at 600°C.*

The particle size is suggested to have direct impact on the rate-limiting steps of CNT growth. The catalyst support will change the crystallographic faces exposed and have effect on the surface reactions, which will influence the growth rate but is not dominating.

4.4 Controlled synthesis of different carbon nanostructures (Paper 7)

Paper 7 presents the synthesis of different carbon nanostructures on powder Fe and Fe/Al_2O_3 catalysts from the decomposition of different carbon containing gases of CO/H_2, CO, CH_4, and C_2H_6/H_2. The effect of catalyst support and reactants on the yield and structure of carbon growth have been studied. From Table 4.3 it is clear that the carbon yield was higher on the powder Fe catalyst from CO disproportionation, but the yield was higher on Fe/Al_2O_3 from hydrocarbons. Completely different or similar structures were synthesized, depending on the gas precursors (Table 4.3).

Table 4.3. *Carbon productivity[a] and structure[b] from different carbon containing gases.*

Reactants	Productivity Fe_3O_4	Productivity Fe/Al_2O_3	Structure Fe_3O_4	Structure Fe/Al_2O_3
CO/H_2	28.8 (171)[c]	17.6 (62)[d]	Platelet	F-T
CO	1.8	1.1[e]	Onion, CNT	Onion, CNT
CH_4	0.37	1.5	Onion, CNT	CNT, Onion
C_2H_6/H_2	0.45	2.24	CNT, F-T	CNT, F-T

[a]Carbon productivity after 8.5 hrs growth, unit: gC/gcat; [b]The structure underlined is the dominating form; F-T: fishbone-tubular; [c]Value in the parenthesis gives the productivity after 50.5 hrs growth; [d]Value in the parenthesis gives the productivity after 30 hrs growth; [e]Complete deactivation after 4 h.

The catalyst activity and the structure of the carbon deposits have been attributed to the size and crystallographic faces of the catalyst particles, which in turn are a direct consequence of the strength of metal-support interaction, and are further influenced by the reactants. Hydrogen plays an essential role in the growth processes by surface reconstruction, keeping the surface clean of carbon, and satisfying dangling bonds.

Controlled synthesis of platelet fibers, fishbone-tubular fibers, onion-like carbon, and CNTs with high quality and selectivity has been realized in this study (Figure 4.8). These different carbon nanostructures will have applications in different fields.

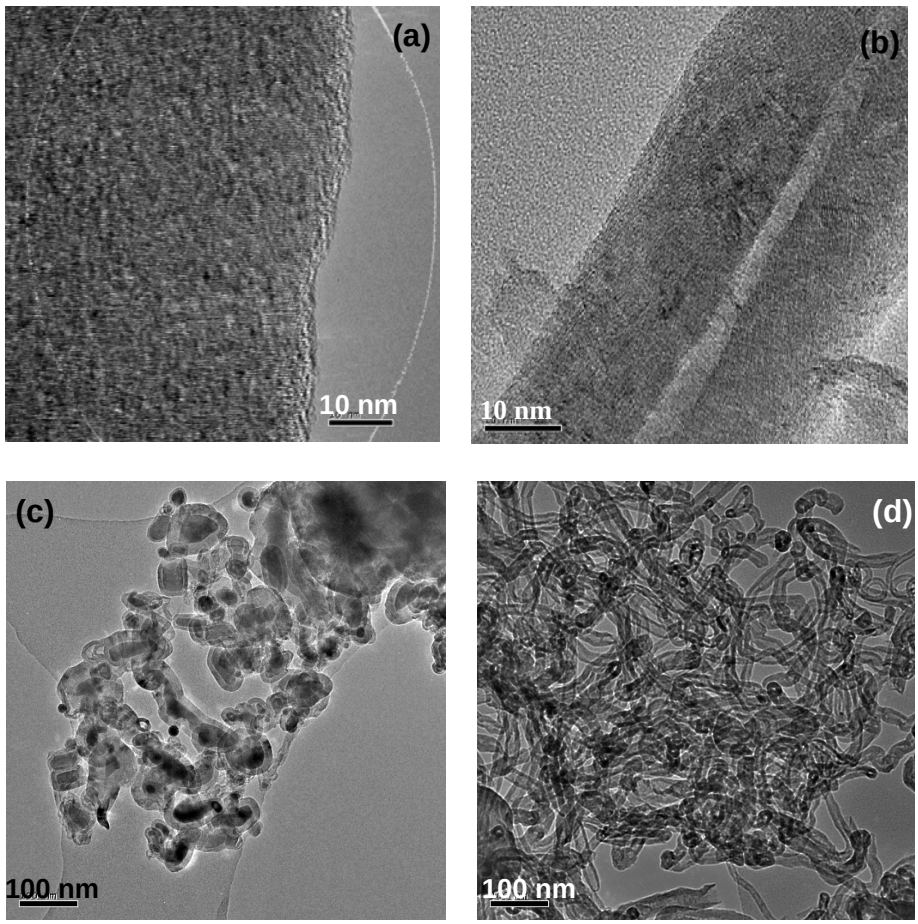

Figure 4.8. *(a) high resolution TEM image shows the platelet structure produced on Fe powder at 600 ℃ from CO/H_2 (40/10); (b) high resolution TEM image shows the fishbone-tubular structure produced over Fe/Al_2O_3 at 600 ℃ from CO/H_2 (40/10); (c) low resolution image of onion-like carbon over Fe powder at 600 ℃ from CO (40); (d) low resolution image shows uniform CNTs produced over Fe powder at 600 ℃ from C_2H_6/H_2 (30/50).*

CONCLUDING REMARKS

The formation of CNFs/CNTs is a very complicated process. Any parameters, such as catalyst precursor, catalyst composition, catalyst metal loading, catalyst support, metal particle size, reaction temperature, gas precursors, gas space velocity, hydrogen concentration, or even reaction time can have a significant impact on the structure, yield, and quality of the CNFs/CNTs.

It is always desirable to get a high carbon productivity with the control of fiber quality and structures. However, this study demonstrated that it is hardly possible to achieve the two outcomes at the same time. Take HT derived Ni/Al_2O_3 (77.5 wt.%) catalyst as an example, it can achieve a very high productivity (50 gCNF/gcat in 5.3 h) from ethylene decomposition with reasonably good structure and diameter distribution. However, the structure and diameter distribution are never as uniform as CNFs produced on 20 wt.% Ni/Al_2O_3 catalyst from ethylene. Unfortunately, this latter supported catalyst can only have a productivity of 5 gCNF/gcat in 8 h. It is also possible to obtain very uniform structures on 77.5 wt.% Ni/Al_2O_3 catalyst, but then a low reactive gas such as methane has to be used. Nevertheless, the productivity from methane is again inherently lower (22 gCNF/gcat in 12 h). Consequently, a comprise has to be made. A recurring theme throughout this study is that there is always a comprise between CNF/CNT productivity and quality, which can be optimized by careful choices of the above parameters.

An important contribution from this study is that the effect of the catalyst particle size in the growth of CNTs has been explicitly demonstrated. Therefore, any treatment processes that have potential impact on the metal particle sizes, such as calcination or reduction, might influence the growth rate.

REFERENCES

[1] H.W. Kroto, J.R. Heath, S.C. Obrien, R.F. Curl, R.E. Smalley, Nature 318 (1985) 162.
[2] S. Iijima, Nature 354 (1991) 56.
[3] S. Iijima, T. Ichihashi, Nature 363 (1993) 603.
[4] M. Endo, Chemtech 18 (1988) 568.
[5] M. Endo, Y.A. Kim, T. Hayashi, K. Nishimura, T. Matusita, K. Miyashita, M.S. Dresselhaus, Carbon 39 (2001) 1287.
[6] M. Endo, Y.A. Kim, T. Takeda, S.H. Hong, T. Matusita, T. Hayashi, M.S. Dresselhaus, Carbon 39 (2001) 2003.
[7] B.I. Yakobson, R.E. Smalley, Am. Sci. 85 (1997) 324.
[8] M. Endo, Y.A. Kim, T. Matusita, T. Hayashi, in L.P. Biro, C.A. Bernardoca, G.G. Tibbetts, Ph. Lambin (Ed.), Carbon Filaments and Nanotubes: Common Origins, Differing Applications? Kluwer Academic Publishers, Dordrecht, 2001, p. 51.
[9] D.S. Tang, S.S. Xie, W. Liu, B.H. Chang, L.F. Sun, Z.Q. Liu, G. Wan, W.Y. Zhou, Carbon 38 (2000) 480.
[10] T.W. Ebbesen, P.M. Ajayan, Nature 358 (1992) 220.
[11] D.S. Bethune, C.H. Kiang, M.S. Devries, G. Gorman, R. Savoy, J. Vazquez, R. Beyers, Nature 363 (1993) 605.
[12] A. Thess, R. Lee, P. Nikolaev, H.J. Dai, P. Petit, J. Robert, C.H. Xu, Y.H. Lee, S.G. Kim, A.G. Rinzler, D.T. Colbert, G.E. Scuseria, D. Tomanek, J.E. Fischer, R.E. Smalley, Science 273 (1996) 483.
[13] R. Marangoni, P. Serp, R. Feurer, Y. Kihn, P. Kalck, C. Vahlas, Carbon 39 (2001) 443.
[14] J.R. Nielsen, D.L. Trimm, J. Catal. 48 (1977) 155.
[15] D.L. Trimm, Catal. Rev. - Sci. Eng. 16 (1977) 155.
[16] C.H. Bartholomew, Catal. Rev. - Sci. Eng. 24 (1982) 67.
[17] R.T.K. Baker, Carbon 27 (1989) 315.
[18] N.M. Rodriguez, J. Mater. Res. 8 (1993) 3233.
[19] K.P. De Jong, J.W. Geus, Catal. Rev. - Sci. Eng. 42 (2000) 481.
[20] V.V. Chesnokov, R.A. Buyanov, Russ. Chem. Rev. 69 (2000) 623.
[21] H.J. Dai, in M.S. Dresselhaus, G. Dresselhaus, Ph. Avouris (Ed.), Carbon Nanotubes: Synthesis, Structure, Properties, and Applications, Springer-Verlag, Heidelberg, 2001, p. 29.
[22] H.J. Dai, Acc. Chem. Res. 35 (2002) 1035.
[23] H.J. Dai, Surf. Sci. 500 (2002) 218.
[24] A. Huczko, Appl. Phys. A 74 (2002) 617.
[25] P.M. Ajayan, Chem. Rev. 99 (1999) 1787.
[26] O. Zhou, H. Shimoda, B. Gao, S.J. Oh, L. Fleming, G.Z. Yue, Acc. Chem. Res. 35 (2002) 1045.
[27] V.N. Popov, Mater. Sci. Eng. R 43 (2004) 61.
[28] C.N.R. Rao, B.C. Satishkumar, A. Govindaraj, M. Nath, Chemphyschem 2 (2001) 78.
[29] C.N.R. Rao, A. Govindaraj, Acc. Chem. Res. 35 (2002) 998.
[30] M. Meyyappan, L. Delzeit, A. Cassell, D. Hash, Plasma Sources Sci. T. 12 (2003) 205.
[31] T.W. Ebbesen, Annu. Rev. Mater. Sci. 24 (1994) 235.

[32] D.T. Colbert, R.E. Smalley, in E. Osawa (Ed.), Perspectives of Fullerene Nanotechnology, Kluwer Academic Publishers, 2002, p. 3.
[33] M. Terrones, W.K. Hsu, H.W. Kroto, D.R.M. Walton, in Fullerenes and Related Structures, 199 (1999) 189.
[34] R.H. Baughman, A.A. Zakhidov, W.A. de Heer, Science 297 (2002) 787.
[35] R. Saito, G. Dresselhaus, M.S. Dresselhaus, Physical Properties of Carbon Nanotubes, Imperial College Press, London, 1998.
[36] P.J.F. Harris, Carbon Nanotubes and Related Structures: New Materials for the Twenty-first Century, Cambridge University Press, Cambridge, 1999.
[37] K. Tanaka, T. Yamabe, K. Fukui (Ed.), The science and Technology of Carbon Nanotubes, Elsevier Science Ltd, Oxford, 1999.
[38] M.S. Dresselhaus, G. Dresselhaus, Ph. Avouris (Ed.), Carbon Nanotubes: Synthesis, Structure, Properties, and Applications, Springer-Verlag, Heidelberg, 2001.
[39] L.P. Biro, C.A. Bernardoca, G.G. Tibbetts, Ph. Lambin (Ed.), Carbon Filaments and Nanotubes: Common Origin, Differing Applications? Kluwer Academic Publishers, Dordrecht, 2001.
[40] M.S. Kim, N.M. Rodriguez, R.T.K. Baker, J. Catal. 131 (1991) 60.
[41] N.M. Rodriguez, M.S. Kim, R.T.K. Baker, J. Catal. 144 (1993) 93.
[42] A. Chambers, N.M. Rodriguez, R.T.K. Baker, J. Mater. Res. 11 (1996) 430.
[43] N. Krishnankutty, N.M. Rodriguez, R.T.K. Baker, J. Catal. 158 (1996) 217.
[44] C. Park, N.M. Rodriguez, R.T.K. Baker, J. Catal. 169 (1997) 212.
[45] C. Park, R.T.K. Baker, J. Catal. 179 (1998) 361.
[46] C. Park, R.T.K. Baker, J. Catal. 190 (2000) 104.
[47] P.E. Anderson, N.M. Rodriguez, J. Mater. Res. 14 (1999) 2912.
[48] C. Park, M.A. Keane, Langmuir 17 (2001) 8386.
[49] P.E. Anderson, N.M. Rodriguez, Chem. Mater. 12 (2000) 823.
[50] P.E. Anderson, E. Engel, A. Crowe, C. Park, N.M. Rodriguez, in WM'00 Conference, Tuscon, AZ, 2000.
[51] M.A. Ermakova, D.Y. Ermakov, G.G. Kuvshinov, L.M. Plyasova, J. Catal. 187 (1999) 77.
[52] C. Park, M.A. Keane, J. Catal. 221 (2004) 386.
[53] M.A. Ermakova, D.Y. Ermakov, A.L. Chuvilin, G.G. Kuvshinov, J. Catal. 201 (2001) 183.
[54] S. Takenaka, M. Serizawa, K. Otsuka, J. Catal. 222 (2004) 520.
[55] T. de los Arcos, M.G. Garnier, J.W. Seo, P. Oelhafen, V. Thommen, D. Mathys, J. Phys. Chem. B 108 (2004) 7728.
[56] Q.W. Li, H. Yan, Y. Cheng, J. Zhang, Z.F. Liu, J. Mater. Chem. 12 (2002) 1179.
[57] N. Nagaraju, A. Fonseca, Z. Konya, J. B.Nagy, J. Mol. Catal. A 181 (2002) 57.
[58] I. Willems, Z. Konya, A. Fonseca, J. B.Nagy, Appl. Catal. A 229 (2002) 229.
[59] K. Hernadi, Z. Konya, A. Siska, J. Kiss, A. Oszko, J. B.Nagy, I. Kiricsi, Mater. Chem. Phys. 77 (2002) 536.
[60] K. Hernadi, Chem. Phys. Lett. 363 (2002) 169.
[61] C.J. Lee, J. Park, J.A. Yu, Chem. Phys. Lett. 360 (2002) 250.
[62] L. Dong, J. Jiao, C. Pan, D.W. Tuggle, Appl. Phys. A 78 (2004) 9.
[63] Y. Soneda, L. Duclaux, F. Beguin, Carbon 40 (2002) 965.
[64] Z.P. Huang, D.Z. Wang, J.G. Wen, M. Sennett, H. Gibson, Z.F. Ren, Appl. Phys. A 74 (2002) 387.
[65] N.M. Rodriguez, A. Chambers, R.T.K. Baker, Langmuir 11 (1995) 3862.

[66] I. Willems, Z. Konya, J.F. Colomer, G. Van Tendeloo, N. Nagaraju, A. Fonseca, J. B.Nagy, Chem. Phys. Lett. 317 (2000) 71.
[67] S. Takenaka, Y. Shigeta, E. Tanabe, K. Otsuka, J. Catal. 220 (2003) 468.
[68] G. Luo, Z. Li, F. Wei, L. Xiang, X. Deng, Y. Ji, Physica B 323 (2002) 314.
[69] X.Z. Liao, A. Serquis, Q.X. Jia, D.E. Peterson, Y.T. Zhu, H.F. Xu, Appl. Phys. Lett. 82 (2003) 2694.
[70] P. Serp, A. Madronero, J.L. Figueiredo, Fuel 78 (1999) 837.
[71] K. Hernadi, A. Fonseca, P. Piedigrosso, M. Delvaux, J. B.Nagy, D. Bernaerts, J. Riga, Catal. Lett. 48 (1997) 229.
[72] K. Hernadi, A. Fonseca, J. B.Nagy, A. Siska, I. Kiricsi, Appl. Catal. A 199 (2000) 245.
[73] R.L. Vander Wal, L.J. Hall, Chem. Phys. Lett. 349 (2001) 178.
[74] M.L. Toebes, J.H. Bitter, A.J. van Dillen, K.P. de Jong, Catal. Today 76 (2002) 33.
[75] K. Otsuka, S. Kobayashi, S. Takenaka, Appl. Catal. A 210 (2001) 371.
[76] A. Kukovecz, Z. Konya, N. Nagaraju, I. Willems, A. Tamasi, A. Fonseca, J. B.Nagy, I. Kiricsi, Phys. Chem. Chem. Phys. 2 (2000) 3071.
[77] S. Takenaka, S. Kobayashi, H. Ogihara, K. Otsuka, J. Catal. 217 (2003) 79.
[78] D. Venegoni, P. Serp, R. Feurer, Y. Kihn, C. Vahlas, P. Kalck, Carbon 40 (2002) 1799.
[79] W.Z. Li, J.G. Wen, Z.F. Ren, Appl. Phys. A 74 (2002) 397.
[80] C. Singh, M.S. Shaffer, A.H. Windle, Carbon 41 (2003) 359.
[81] C. Ducati, I. Alexandrou, M. Chhowalla, G.A.J. Amaratunga, J. Robertson, J. Appl. Phys. 92 (2002) 3299.
[82] I. Alstrup, M.T. Tavares, C.A. Bernardo, O. Sorensen, J.R. Rostrup-Nielsen, Mater. Corros. 49 (1998) 367.
[83] C.J. Lee, J. Park, Y. Huh, J.Y. Lee, Chem. Phys. Lett. 343 (2001) 33.
[84] K. Hernadi, A. Gaspar, J.W. Seo, M. Hammida, A. Demortier, L. Forro, J. B.Nagy, I. Kiricsi, Carbon 42 (2004) 1599.
[85] A. Peigney, C. Laurent, A. Rousset, J. Mater. Chem. 9 (1999) 1167.
[86] W.F. Liu, W.L. Cai, L.Z. Yao, X.G. Li, Z. Yao, J. Mater. Sci. 38 (2003) 3051.
[87] S.C. Lyu, B.C. Liu, T.J. Lee, Z.Y. Liu, C.W. Yang, C.Y. Park, C.J. Lee, Chem. Commun. (2003) 734.
[88] W.Z. Li, J.G. Wen, Y. Tu, Z.F. Ren, Appl. Phys. A 73 (2001) 259.
[89] P. Pinheiro, M.C. Schouler, P. Gadelle, M. Mermoux, E. Dooryhee, Carbon 38 (2000) 1469.
[90] H. Neumayer, R. Haubner, Diam. Relat. Mater. 13 (2004) 1191.
[91] K. Bladh, L.K.L. Falk, F. Rohmund, Appl. Phys. A 70 (2000) 317.
[92] J. Jiao, P.E. Nolan, S. Seraphin, A.H. Cutler, D.C. Lynch, J. Electrochem. Soc. 143 (1996) 932.
[93] J. Jiao, S. Seraphin, Chem. Phys. Lett. 249 (1996) 92.
[94] P.E. Nolan, D.C. Lynch, A.H. Cutler, Carbon 32 (1994) 477.
[95] P.E. Nolan, M.J. Schabel, D.C. Lynch, A.H. Cutler, Carbon 33 (1995) 79.
[96] P.E. Nolan, D.C. Lynch, A.H. Cutler, J. Phys. Chem. B 102 (1998) 4165.
[97] S. Takenaka, H. Ogihara, K. Otsuka, J. Catal. 208 (2002) 54.
[98] K. Otsuka, H. Ogihara, S. Takenaka, Carbon 41 (2003) 223.
[99] E.F. Kukovitsky, S.G. L'Vov, N.A. Sainov, V.A. Shustov, L.A. Chernozatonskii, Chem. Phys. Lett. 355 (2002) 497.
[100] M. Perez-Cabero, I. Rodriguez-Ramos, A. Guerrero-Ruiz, J. Catal. 215 (2003) 305.

[101] P.M. Ajayan, Nature 427 (2004) 402.
[102] R.T.K. Baker, P.S. Harris, R.B. Thomas, R.J. Waite, J. Catal. 30 (1973) 86.
[103] P. Chitrapu, C.R.F. Lund, J.A. Tsamopoulos, Carbon 30 (1992) 285.
[104] P. Wang, E. Tanabe, K. Ito, J. Jia, H. Morioka, T. Shishido, K. Takehira, Appl. Catal. A 231 (2002) 35.
[105] P. Coquay, R.E. Vandenberghe, E. De Grave, A. Fonseca, P. Piedigrosso, J. B.Nagy, J. Appl. Phys. 92 (2002) 1286.
[106] O.A. Nerushev, S. Dittmar, R.E. Morjan, F. Rohmund, E.E.B. Campbell, J. Appl. Phys. 93 (2003) 4185.
[107] H. Yan, Q.W. Li, J. Zhang, Z.F. Liu, Carbon 40 (2002) 2693.
[108] V. Jourdain, O. Stephan, M. Castignolles, A. Loiseau, P. Bernier, Adv. Mater. 16 (2004) 447.
[109] Y.Y. Fan, H.M. Cheng, Y.L. Wei, G. Su, Z.H. Shen, Carbon 38 (2000) 921.
[110] Y.Y. Fan, H.M. Cheng, Y.L. Wei, G. Su, Z.H. Shen, Carbon 38 (2000) 789.
[111] S.C. Lyu, B.C. Liu, S.H. Lee, C.Y. Park, H.K. Kang, C.W. Yang, C.J. Lee, J. Phys. Chem. B 108 (2004) 1613.
[112] B. Zheng, Y. Li, J. Liu, Appl. Phys. A 74 (2002) 345.
[113] M. Su, B. Zheng, J. Liu, Chem. Phys. Lett. 322 (2000) 321.
[114] M.J. Bronikowski, P.A. Willis, D.T. Colbert, K.A. Smith, R.E. Smalley, J. Vac. Sci. Technol. A 19 (2001) 1800.
[115] Y. Li, J. Liu, Y.Q. Wang, Z.L. Wang, Chem. Mater. 13 (2001) 1008.
[116] A.M. Cassell, J.A. Raymakers, J. Kong, H.J. Dai, J. Phys. Chem. B 103 (1999) 6484.
[117] B. Zheng, C.G. Lu, G. Gu, A. Makarovski, G. Finkelstein, J. Liu, Nano Lett. 2 (2002) 895.
[118] B.C. Liu, S.C. Lyu, T.J. Lee, S.K. Choi, S.J. Eum, C.W. Yang, C.Y. Park, C.J. Lee, Chem. Phys. Lett. 373 (2003) 475.
[119] H. Ago, S. Ohshima, K. Uchida, M. Yumura, J. Phys. Chem. B 105 (2001) 10453.
[120] W.E. Alvarez, B. Kitiyanan, A. Borgna, D.E. Resasco, Carbon 39 (2001) 547.
[121] B. Kitiyanan, W.E. Alvarez, J.H. Harwell, D.E. Resasco, Chem. Phys. Lett. 317 (2000) 497.
[122] D.E. Resasco, W.E. Alvarez, F. Pompeo, L. Balzano, J.E. Herrera, B. Kitiyanan, A. Borgna, J. Nanopart. Res. 4 (2002) 131.
[123] Y.M. Li, W. Kim, Y.G. Zhang, M. Rolandi, D.W. Wang, H.J. Dai, J. Phys. Chem. B 105 (2001) 11424.
[124] J.M. Bonard, P. Chauvin, C. Klinke, Nano Lett. 2 (2002) 665.
[125] Y.M. Li, D. Mann, M. Rolandi, W. Kim, A. Ural, S. Hung, A. Javey, J. Cao, D.W. Wang, E. Yenilmez, Q. Wang, J.F. Gibbons, Y. Nishi, H.J. Dai, Nano Lett. 4 (2004) 317.
[126] J.F. Geng, C. Singh, D.S. Shephard, M.S.P. Shaffer, B.F.G. Johnson, A.H. Windle, Chem. Commun. (2002) 2666.
[127] A.C. Dillon, A.H. Mahan, P.A. Parilla, J.L. Alleman, M.J. Heben, K.M. Jones, K.E.H. Gilbert, Nano Lett. 3 (2003) 1425.
[128] A.R. Harutyunyan, B.K. Pradhan, U.J. Kim, G.G. Chen, P.C. Eklund, Nano Lett. 2 (2002) 525.
[129] M.H. Hu, Y. Murakami, M. Ogura, S. Maruyama, T. Okubo, J. Catal. 225 (2004) 230.
[130] J.E. Herrera, L. Balzano, A. Borgna, W.E. Alvarez, D.E. Resasco, J. Catal. 204 (2001) 129.

[131] J.E. Herrera, D.E. Resasco, J. Catal. 221 (2004) 354.
[132] J.E. Herrera, D.E. Resasco, J. Phys. Chem. B 107 (2003) 3738.
[133]J.F. Colomer, C. Stephan, S. Lefrant, G. Van Tendeloo, I. Willems, Z. Konya, A. Fonseca, C. Laurent, J. B.Nagy, Chem. Phys. Lett. 317 (2000) 83.
[134]B.C. Liu, S.C. Lyu, S.I. Jung, H.K. Kang, C.W. Yang, J.W. Park, C.Y. Park, C.J. Lee, Chem. Phys. Lett. 383 (2004) 104.
[135] P. Nikolaev, J. Nanosci. Nanotechnol. 4 (2004) 307.
[136] K. Hata, D.N. Futaba, K. Mizuno, T. Namai, M. Yumura, S. Iijima, Science 306 (2004) 1362.
[137] G.G. Tibbetts, J. Cryst. Growth 66 (1984) 632.
[138] J. B.Nagy, G. Bister, A. Fonseca, D. Mehn, Z. Konya, I. Kiricsi, Z.E. Horvath, L.P. Biro, J. Nanosci. Nanotechnol. 4 (2004) 326.
[139] D.E. Resasco, J.E. Herrera, L. Balzano, J. Nanosci. Nanotechnol. 4 (2004) 398.
[140] S. Helveg, C. Lopez-Cartes, J. Sehested, P.L. Hansen, B.S. Clausen, J.R. Rostrup-Nielsen, F. Abild-Pedersen, J.K. Norskov, Nature 427 (2004) 426.
[141] A.N. Andriotis, M. Menon, G. Froudakis, Phys. Rev. Lett. 85 (2000) 3193.
[142] H.J. Dal, A.G. Rinzler, P. Nikolaev, A. Thess, D.T. Colbert, R.E. Smalley, Chem. Phys. Lett. 260 (1996) 471.
[143] W. Teunissen, Ph.D. Thesis, Utrecht University, The Nethelands, 2000.
[144] A.K. Schaper, H.Q. Hou, A. Greiner, F. Phillipp, J. Catal. 222 (2004) 250.
[145] V.L. Kuznetsov, A.N. Usoltseva, A.L. Chuvilin, E.D. Obraztsova, J.M. Bonard, Phys. Rev. B 64 (2001).
[146] J. Gavillet, A. Loiseau, F. Ducastelle, S. Thair, P. Bernier, O. Stephan, J. Thibault, J.C. Charlier, Carbon 40 (2002) 1649.
[147] J. Gavillet, A. Loiseau, C. Journet, F. Willaime, F. Ducastelle, J.C. Charlier, Phys. Rev. Lett. 87 (2001).
[148] J. Gavillet, J. Thibault, O. Stephan, H. Amara, A. Loiseau, C. Bichara, J.P. Gaspard, F. Ducastelle, J. Nanosci. Nanotechnol. 4 (2004) 346.
[149] A. Gorbunov, O. Jost, W. Pompe, A. Graff, Carbon 40 (2002) 113.
[150] O. Jost, A. Gorbunov, X.J. Liu, W. Pompe, J. Fink, J. Nanosci. Nanotechnol. 4 (2004) 433.
[151] J.H. Hafner, M.J. Bronikowski, B.R. Azamian, P. Nikolaev, A.G. Rinzler, D.T. Colbert, K.A. Smith, R.E. Smalley, Chem. Phys. Lett. 296 (1998) 195.
[152] J.W. Snoeck, G.F. Froment, M. Fowles, J. Catal. 169 (1997) 240.
[153] Y.H. Hu, E. Ruckenstein, J. Catal. 184 (1999) 298.
[154] Y.J. Tian, Z. Hu, Y. Yang, X.Z. Wang, X. Chen, H. Xu, Q. Wu, W.J. Ji, Y. Chen, J. Am. Chem. Soc. 126 (2004) 1180.
[155] A.C. Dillon, K.M. Jones, T.A. Bekkedahl, C.H. Kiang, D.S. Bethune, M.J. Heben, Nature 386 (1997) 377.
[156] A. Chambers, C. Park, R.T.K. Baker, N.M. Rodriguez, J. Phys. Chem. B 102 (1998) 4253.
[157] C. Liu, Y.Y. Fan, M. Liu, H.T. Cong, H.M. Cheng, M.S. Dresselhaus, Science 286 (1999) 1127.
[158] P. Chen, X. Wu, J. Lin, K.L. Tan, Science 285 (1999) 91.
[159] M.S. Dresselhaus, K.A. Williams, P.C. Eklund, MRS Bull. 24 (1999) 45.
[160] S. Orimo, A. Zuttel, L. Schlapbach, G. Majer, T. Fukunaga, H. Fujii, J. Alloys Compd. 356 (2003) 716.
[161] M. Becher, M. Haluska, M. Hirscher, A. Quintel, V. Skakalova, U. Dettlaff-Weglikovska, X. Chen, M. Hulman, Y. Choi, S. Roth, V. Meregalli, M.

Parrinello, R. Strobel, L. Jorissen, M.M. Kappes, J. Fink, A. Zuttel, I. Stepanek, P. Bernierg, C. R. Phys. 4 (2003) 1055.
[162] U. Bunger, W. Zittel, Appl. Phys. A 72 (2001) 147.
[163] F.L. Darkrim, P. Malbrunot, G.P. Tartaglia, Int. J. Hydrogen Energy 27 (2002) 193.
[164] A.C. Dillon, M.J. Heben, Appl. Phys. A 72 (2001) 133.
[165] M. Hirscher, M. Becher, M. Haluska, A. Quintel, V. Skakalova, Y.M. Choi, U. Dettlaff-Weglikowska, S. Roth, I. Stepanek, P. Bernier, A. Leonhardt, J. Fink, J. Alloys Compd. 330 (2002) 654.
[166] V.V. Simonyan, J.K. Johnson, J. Alloys Compd. 330 (2002) 659.
[167] R.G. Ding, G.Q. Lu, Z.F. Yan, M.A. Wilson, J. Nanosci. Nanotechnol. 1 (2001) 7.
[168] R.T. Yang, Carbon 38 (2000) 623.
[169]F.E. Pinkerton, B.G. Wicke, C.H. Olk, G.G. Tibbetts, G.P. Meisner, M.S. Meyer, J.F. Herbst, J. Phys. Chem. B 104 (2000) 9460.
[170]M. Hirscher, M. Becher, M. Haluska, U. Dettlaff-Weglikowska, A. Quintel, G.S. Duesberg, Y.M. Choi, P. Downes, M. Hulman, S. Roth, I. Stepanek, P. Bernier, Appl. Phys. A 72 (2001) 129.
[171] M. Hirscher, M. Becher, M. Haluska, F. von Zeppelin, X.H. Chen, U. Dettlaff-Weglikowska, S. Roth, J. Alloys Compd. 356 (2003) 433.
[172] H.G. Schimmel, G.J. Kearley, M.G. Nijkamp, C.T. Visserl, K.P. de Jong, F.M. Mulder, Chem. - Eur. J. 9 (2003) 4764.
[173] M. Ritschel, M. Uhlemann, O. Gutfleisch, A. Leonhardt, A. Graff, C. Taschner, J. Fink, Appl. Phys. Lett. 80 (2002) 2985.
[174] G.G. Tibbetts, G.P. Meisner, C.H. Olk, Carbon 39 (2001) 2291.
[175] C. Zandonella, Nature 410 (2001) 734.
[176] C. Liu, Q.H. Yang, Y. Tong, H.T. Cong, H.M. Cheng, Appl. Phys. Lett. 80 (2002) 2389.
[177]A. Zuttel, P. Sudan, P. Mauron, T. Kiyobayashi, C. Emmenegger, L. Schlapbach, Int. J. Hydrogen Energy 27 (2002) 203.
[178] A. Zuttel, P. Sudan, P. Mauron, P. Wenger, Appl. Phys. A 78 (2004) 941.
[179] R. Strobel, L. Jorissen, T. Schliermann, V. Trapp, W. Schutz, K. Bohmhammel, G. Wolf, J. Garche, J. Power Sources 84 (1999) 221.
[180] D.J. Browning, M.L. Gerrard, J.B. Lakeman, I.M. Mellor, R.J. Mortimer, M.C. Turpin, Nano Lett. 2 (2002) 201.
[181] A.D. Lueking, R.T. Yang, N.M. Rodriguez, R.T.K. Baker, Langmuir 20 (2004) 714.
[182] W.Q. Deng, X. Xu, W.A. Goddard, Phys. Rev. Lett. 92 (2004) 166103.
[183] A.D. Lueking, R.T. Yang, Appl. Catal. A 265 (2004) 259.
[184] M.A. Callejas, A. Anson, A.M. Benito, W. Maser, J.L.G. Fierro, M.L. Sanjuan, M.T. Martinez, Mater. Sci. Eng. B 108 (2004) 120.
[185] D. Chen, L. Chen, S. Liu, C.X. Ma, D.M. Chen, L.B. Wang, J. Alloys Compd. 372 (2004) 231.
[186] S. Yamanaka, M. Fujikane, M. Uno, H. Murakami, O. Miura, J. Alloys Compd. 366 (2004) 264.
[187]C. Park, P.E. Anderson, A. Chambers, C.D. Tan, R. Hidalgo, N.M. Rodriguez, J. Phys. Chem. B 103 (1999) 10572.
[188] P.X. Hou, Q.H. Yang, S. Bai, S.T. Xu, M. Liu, H.M. Cheng, J. Phys. Chem. B 106 (2002) 963.
[189] A. Lueking, R.T. Yang, AIChE J. 49 (2003) 1556.

[190] G.Q. Ning, F. Wei, G.H. Luo, Q.X. Wang, Y.L. Wu, H. Yu, Appl. Phys. A 78 (2004) 955.
[191] S. Collins, R. Brydson, B. Rand, Carbon 40 (2002) 1089.
[192] C.H. Kiang, M. Endo, P.M. Ajayan, G. Dresselhaus, M.S. Dresselhaus, Phys. Rev. Lett. 81 (1998) 1869.
[193] D. Bom, R. Andrews, D. Jacques, J. Anthony, B.L. Chen, M.S. Meier, J.P. Selegue, Nano Lett. 2 (2002) 615.
[194] L.S.K. Pang, J.D. Saxby, S.P. Chatfield, J. Phys. Chem. 97 (1993) 6941.
[195] T. Shimada, H. Yanase, K. Morishita, J.I. Hayashi, T. Chiba, Carbon 42 (2004) 1635.